Monthly Notices of the ROYAL ASTRONOMICAL SOCIETY

MNRAS **473,** 4956–4974 (2018) doi:10.1093/mnras/stx2667
Advance Access publication 2017 October 14

Quantifying the impact of mergers on the angular momentum of simulated galaxies

Claudia del P. Lagos,[1,2]★ Adam R. H. Stevens,[3] Richard G. Bower,[4] Timothy A. Davis,[5] Sergio Contreras,[6] Nelson D. Padilla,[6,7] Danail Obreschkow,[1,2] Darren Croton,[3] James W. Trayford,[4] Charlotte Welker[1,2] and Tom Theuns[4]

[1]*International Centre for Radio Astronomy Research (ICRAR), M468, University of Western Australia, 35 Stirling Hwy, Crawley, WA 6009, Australia*
[2]*Australian Research Council Centre of Excellence for All-sky Astrophysics (CAASTRO), 44 Rosehill Street Redfern, NSW 2016, Australia*
[3]*Centre for Astrophysics and Supercomputing, Swinburne University of Technology, Hawthorn, VIC 3122, Australia*
[4]*Institute for Computational Cosmology, Department of Physics, University of Durham, South Road, Durham DH1 3LE, UK*
[5]*School of Physics and Astronomy, Cardiff University, Queens Buildings, The Parade, Cardiff CF24 3AA, UK*
[6]*Instituto de Astrofísica, Pontificia Universidad Católica de Chile, Avda. Vicuña Mackenna 4860, 782-0436 Macul, Santiago, Chile*
[7]*Centro de Astro-Ingeniería, Pontificia Universidad Católica de Chile, Avda. Vicuña Mackenna 4860, 782-0436 Macul, Santiago, Chile*

Accepted 2017 October 6. Received 2017 October 6; in original form 2016 December 22

ABSTRACT

We use EAGLE to quantify the effect galaxy mergers have on the stellar specific angular momentum of galaxies, $j_{\rm stars}$. We split mergers into dry (gas-poor)/wet (gas-rich), major/minor and different spin alignments and orbital parameters. Wet (dry) mergers have an average neutral gas-to-stellar mass ratio of 1.1 (0.02), while major (minor) mergers are those with stellar mass ratios $\geq$0.3 (0.1–0.3). We correlate the positions of galaxies in the $j_{\rm stars}$–stellar mass plane at $z = 0$ with their merger history, and find that galaxies of low spins suffered dry mergers, while galaxies of normal/high spins suffered predominantly wet mergers, if any. The radial $j_{\rm stars}$ profiles of galaxies that went through dry mergers are deficient by $\approx$0.3 dex at $r \lesssim 10\, r_{50}$ (with r_{50} being the half-stellar mass radius), compared to galaxies that went through wet mergers. Studying the merger remnants reveals that dry mergers reduce $j_{\rm stars}$ by $\approx$30 per cent, while wet mergers increase it by $\approx$10 per cent, on average. The latter is connected to the build-up of the bulge by newly formed stars of high rotational speed. Moving from minor to major mergers accentuates these effects. When the spin vectors of the galaxies prior to the dry merger are misaligned, $j_{\rm stars}$ decreases by a greater magnitude, while in wet mergers corotation and high orbital angular momentum efficiently spun-up galaxies. We predict what would be the observational signatures in the $j_{\rm stars}$ profiles driven by dry mergers: (i) shallow radial profiles and (ii) profiles that rise beyond $\approx 10\, r_{50}$, both of which are significantly different from spiral galaxies.

Key words: galaxies: evolution – galaxies: formation – galaxies: fundamental parameters – galaxies: structure.

1 INTRODUCTION

Galaxy mergers are a natural consequence of the hierarchical growth of structures (White & Rees 1978) and since early on have been posed to be a key physical process in their morphological transformation (e.g. Toomre & Toomre 1972; Toomre 1977; White 1978; Farouki & Shapiro 1982; Barnes 1988). Since then, galaxy mergers have become an essential process in cosmological galaxy formation models (e.g. Cole et al. 2000; Springel et al. 2001; Bower et al. 2006; De Lucia et al. 2006; Lagos, Cora & Padilla 2008, see Baugh 2006 for a review).

In the context of the angular momentum (AM) of galaxies, Fall (1983) presented the first observational compilation of the specific AM of the stellar component of galaxies, $j_{\rm stars}$ and its relation with stellar mass, $M_{\rm stars}$. Fall (1983) found that elliptical and spiral galaxies follow parallel sequences, with the former having $j_{\rm stars}$ a factor of $\approx$6 lower than the latter. Fall (1983) concluded that in hierarchical cosmologies, the $j_{\rm stars}$ values of spirals and ellipticals could be understood if spirals roughly conserve j in their formation process (see also Mo, Mao & White 1998), while ellipticals suffer efficient j dissipation. Galaxy mergers are a natural dissipative phenomenon which could account for the galaxy population of low spins. Early

★ E-mail: claudia.lagos@icrar.org

simulations (e.g. Barnes & Efstathiou 1987; Navarro & White 1994; Heyl, Hernquist & Spergel 1996; Zavala, Okamoto & Frenk 2008) showed that dynamical friction can efficiently move high j material to the outer regions of galaxies, effectively lowering the $j_{\rm stars}$ of the stellar component that is easily measurable. Later on, Romanowsky & Fall (2012), via idealized models within the Λ cold dark matter paradigm, showed that galaxy mergers can naturally explain the positions of elliptical galaxies in the $j_{\rm stars}$–$M_{\rm stars}$ plane, and that discs and bulges follow fundamentally different $j_{\rm stars}$–$M_{\rm stars}$ relations. Recently, using the EAGLE simulations, Zavala et al. (2016) showed that the AM loss of a galaxy's stellar component follows closely that of the inner parts of its haloes, which would be naturally explained by the merging activity of haloes and galaxies at low redshifts. Using the same simulations, Lagos et al. (2017) found that mergers were not the only ones responsible of small spins, but that galaxies could also have low $j_{\rm stars}$ due to early quenching.

Recent observational measurements of $j_{\rm stars}$ using the Sydney-AAO Multi-object Integral Field Unit (IFU) spectrograph (SAMI; Croom et al. 2012) by Cortese et al. (2016) have suggested that galaxies form a continuous sequence in the $j_{\rm stars}$–$M_{\rm stars}$ plane, instead of the two sequences originally found by Fall (1983). Cortese et al. (2016) found that the positions of galaxies in the $j_{\rm stars}$–$M_{\rm stars}$ plane were strongly correlated with the Hubble morphological type, Sèrsic index and the spin parameter of the stars $\lambda_{\rm R}$, which provides a measurement of how rotationally supported a galaxy is (Emsellem et al. 2007). Cortese et al. (2016) concluded that the large-scale morphology of galaxies is regulated by their mass and dynamical state. Similarly, Obreschkow & Glazebrook (2014) showed that the relation between the disc j and the mass has a scatter that correlates with the bulge-to-total mass ratio, arguing that the physical processes giving rise to the bulge also affect the formation of the disc, and thus there may not be a fundamental distinction between bulges and discs. It is unclear though how much of this result is driven by the sample being dominated by pseudo rather than classic bulges.

This may not, however, be the full story. Emsellem et al. (2011) showed that early-type galaxies, from the ATLAS$^{\rm 3D}$ survey, have a large variety of $\lambda_{\rm R}$ values, and thus, they cannot be seen as one uniform type of galaxy. Emsellem et al. (2011) found two broad classifications for early-type galaxies: fast and slow rotators. Some important trends found by Emsellem et al. (2011) and extended recently to higher stellar masses by Veale et al. (2017) are that the fraction of slow rotators increases steeply with stellar mass and that the vast majority of S0 galaxies are fast rotators. All these observations measure kinematics of galaxies within a relatively small area of the galaxy (typically 1 effective radius), which leaves open the question of whether galaxies with low spins are the result of a major loss of total $j_{\rm stars}$ or simply a rearrangement of $j_{\rm stars}$ in spite of total j conservation. These formation scenarios are not mutually exclusive, and thus, one has to ask what gives rise to such variety of observed dynamical states in galaxies, and particularly, early types.

Jesseit et al. (2009), Bois et al. (2011) and Naab et al. (2014) found that the formation paths of slow and fast rotators can be very varied. For example, Naab et al. (2014) showed that slow rotators could be formed as a result of wet major mergers, dry major mergers and dry minor mergers. In the case of wet mergers, the remnant can be either fast or slow rotators, or even discs (e.g. Bekki 1998; Springel 2000; Cox et al. 2006; Robertson et al. 2006; Johansson, Naab & Burkert 2009; Lotz et al. 2010; Peirani et al. 2010; Naab et al. 2014; Moreno et al. 2015; Sparre & Springel 2016). Di Matteo et al. (2009) showed that even dry major mergers of pressure-supported galaxies can result in a rotation-supported disc if the orbital AM is large enough and efficiently transferred into the orbits of stars. Many of these mergers may result in a dramatic change in the morphology and spin of galaxies, but ultimately mergers are one of many physical processes at play, and continuing gas accretion and star formation can reshape the remnant morphology and kinematics. Recently, using cosmological hydrodynamical simulations, Sparre & Springel (2017) found that galaxy remnants of major mergers evolve into star-forming disc galaxies unless sufficiently strong feedback is present to prevent the disc regrowth. This feedback is an essential mechanism in the new generation of cosmological hydrodynamical simulations, such as EAGLE (Schaye et al. 2015), Illustris (Vogelsberger et al. 2014) and HORIZON-AGN (Dubois et al. 2014), and most likely plays a major role in reproducing the morphological diversity seen in galaxies (Dubois et al. 2016; Correa et al. 2017).

Although there is extensive literature for how different merger configurations can affect galaxies, cosmological hydrodynamical simulations are necessary to realistically represent their frequency in a galaxy population, and thus, it is the best way of shedding light on why galaxies display the diversity of $j_{\rm stars}$ seen in observations, especially as modern simulations reproduce the observations well (Genel et al. 2015; Pedrosa & Tissera 2015; Teklu et al. 2015; Zavala et al. 2016; Lagos et al. 2017; Sokolowska et al. 2017). This is the motivation of this work. We use the EAGLE (Schaye et al. 2015) cosmological hydrodynamical simulations to statistically study how galaxy mergers drive the positions of galaxies in the $j_{\rm stars}$–$M_{\rm stars}$ plane. We also study the main parameters determining how much spin-up or spin-down occurs, and the cumulative effect mergers may have in the $z = 0$ galaxy population. EAGLE has a good compromise between volume, $(100\,{\rm Mpc})^3$, and resolution, 700 pc, that allows us to have a statistically significant sample of galaxies (several thousands with $M_{\rm star} > 10^9\,{\rm M}_\odot$) and with enough structural details to be able to study mean radial $j_{\rm stars}$ profiles.

EAGLE has now been extensively tested against local and high-redshift observations of galaxy sizes (Furlong et al. 2017), colours (Trayford et al. 2015), stellar masses and star formation rates (Furlong et al. 2015; Schaye et al. 2015), and the gas contents of galaxies (Lagos et al. 2015, 2016; Bahé et al. 2016; Crain et al. 2017), among other properties, with high success. This gives us some confidence that we can use EAGLE to learn about the role of galaxy mergers in the $j_{\rm stars}$–$M_{\rm stars}$ plane. The advent of IFU surveys, such as SAMI, MaNGA (Bundy et al. 2015) and MUSE (Bacon et al. 2010), and the first global measurements of $j_{\rm stars}$ at high redshift (Burkert et al. 2016; Harrison et al. 2017; Swinbank et al. 2017) make our study very timely. Previous work studying AM in EAGLE has focused on the galaxy/halo connection (Zavala et al. 2016), the star formation history effect on the AM (Lagos et al. 2017) and the structure of the AM and cooling gas in star-forming galaxies (Stevens et al. 2017). In this paper, we therefore present an independent, but complementary study of AM in galaxies.

This paper is organized as follows. Section 2 briefly describes the EAGLE simulation and introduces the parameters of mergers we study. Here, we also present a comparison with observational measurements of merger rates, to show that the frequency of mergers is well represented in EAGLE. In Section 3, we study the cumulative effect of galaxy mergers as seen by dissecting the $z = 0$ galaxy population. We also compare the mean radial $j_{\rm stars}$ profiles in EAGLE with observations of early-type galaxies. We then focus on the effect galaxy mergers have on the net value of $j_{\rm stars}$ as well as its radial distribution in galaxies, splitting mergers into minor/major, wet/dry and in spin and orbital parameters. Here, we also connect the change in $j_{\rm stars}$ with changes in the stellar mass distribution, and analyse the distribution of the stellar components of the galaxies

Table 1. Features of the Ref-L100N1504 EAGLE simulation used in this paper. The row list: (1) comoving box size, (2) number of particles, (3) initial particle masses of gas and (4) dark matter, (5) comoving gravitational softening length and (6) maximum physical comoving Plummer-equivalent gravitational softening length. Units are indicated in each row. EAGLE adopts (5) as the softening length at $z \geq 2.8$, and (6) at $z < 2.8$.

	Property	Units	Value
(1)	L	cMpc	100
(2)	# particles		2×1504^3
(3)	Gas particle mass	$M_\odot$	1.81×10^6
(4)	DM particle mass	$M_\odot$	9.7×10^6
(5)	Softening length	ckpc	2.66
(6)	Max. gravitational softening	pkpc	0.7

prior to the merger and in the remnant. We present a discussion of our results and our main conclusions in Section 4. Finally, in Appendix A we present a convergence study to show that $j_{\rm stars}$ is well converged for the purpose of our study; in Appendix B we analyse the robustness of our result against the time resolution of the main simulation used here, while Appendix C presents additional plots that aid the interpretation of our results.

2 THE EAGLE SIMULATION

The EAGLE simulation suite (Schaye et al. 2015, hereafter S15, and Crain et al. 2015, hereafter C15) consists of a large number of cosmological hydrodynamic simulations with different resolutions, volumes and subgrid models, adopting the Planck Collaboration XVI (2014) cosmology. S15 introduced a reference model, within which the parameters of the subgrid models governing energy feedback from stars and accreting black holes (BHs) were calibrated to ensure a good match to the $z = 0.1$ galaxy stellar mass function, the sizes of present-day disc galaxies and the BH–stellar mass relation (see C15 for details).

In Table 1, we summarize the parameters of the simulation used in this work. Throughout the text, we use pkpc to denote proper kiloparsecs and cMpc to denote comoving megaparsecs. A major aspect of the EAGLE project is the use of state-of-the-art subgrid models that capture unresolved physics. The subgrid physics modules adopted by EAGLE are (i) radiative cooling and photoheating, (ii) star formation, (iii) stellar evolution and enrichment, (iv) stellar feedback and (v) BH growth and active galactic nucleus (AGN) feedback. In addition, the fraction of atomic and molecular gas in each gas particle is calculated in post-processing following Lagos et al. (2015).

The EAGLE simulations were performed using an extensively modified version of the parallel *N*-body smoothed particle hydrodynamics (SPH) code GADGET-3 (Springel 2005; Springel et al. 2008). Among those modifications are updates to the SPH technique, which are collectively referred to as 'Anarchy' (see Schaller et al. 2015b, for an analysis of the impact of these changes on the properties of simulated galaxies compared to standard SPH). We use SUBFIND (Springel et al. 2001; Dolag et al. 2009) to identify self-bound overdensities of particles within haloes (i.e. substructures). These substructures are the galaxies in EAGLE.

2.1 Merger parameters studied

We identify mergers using the merger trees available in the EAGLE data base (McAlpine et al. 2016). These merger trees were created using the `D-Trees` algorithm of Jiang et al. (2014). Qu et al. (2017) described how this algorithm was adapted to work with EAGLE outputs. Galaxies that went through mergers have more than one progenitor, and for our purpose, we track the most massive progenitors of merged galaxies and compare the properties of those with that of the merger remnant to analyse the effect on $j_{\rm stars}$. The trees stored in the public data base of EAGLE connect 29 epochs. The time span between snapshots can range from ≈0.3 to ≈1 Gyr. We use these snapshots to analyse the evolution of $j_{\rm stars}$ in galaxies and the effect of mergers. We consider the interval between outputs appropriate, as our purpose is to analyse galaxies before and after, rather than during the merger. We study the robustness of our analysis to the time interval between outputs used in the simulations in Appendix B using much finer time intervals (i.e. snipshots; S15). We find that our calculations are robust and do not sensitively depend on how fine the time interval between outputs are.

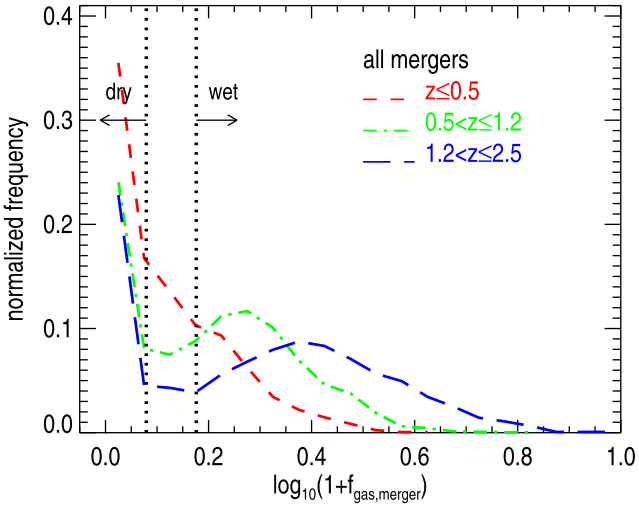

Figure 1. The distribution of the neutral gas-to-stellar mass ratio of mergers in EAGLE in three redshift bins, as labelled. Distributions are mostly bimodal, and we use this to define gas-rich (wet) and gas-poor (dry) mergers in EAGLE (shown as dotted lines).

We split mergers into major and minor mergers. The former are those with a stellar mass ratio between the secondary and the primary galaxy ≥0.3, while minor mergers have a mass ratio between 0.1 and 0.3. Lower mass ratios are considered unresolved and thus are classified as accretion (Crain et al. 2017).

In addition to defining minor and major mergers, we estimate the ratio of gas to stellar mass of the merger with the aim of classifying them as gas-rich (wet) or gas-poor (dry) mergers. This ratio is defined as

$$f_{\rm gas,merger} \equiv \frac{M^{\rm s}_{\rm neutral} + M^{\rm p}_{\rm neutral}}{M^{\rm s}_{\rm stars} + M^{\rm p}_{\rm stars}}, \quad (1)$$

where $M^{\rm s}_{\rm neutral}$ and $M^{\rm p}_{\rm neutral}$ are the neutral gas masses of the secondary and primary galaxies, respectively, while $M^{\rm s}_{\rm stars}$ and $M^{\rm p}_{\rm stars}$ are the corresponding stellar masses. Masses are measured within an aperture of 30 pkpc. Neutral gas fractions of individual particles in EAGLE are calculated as in Lagos et al. (2015). Here, neutral gas refers to atomic plus molecular gas.

Fig. 1 shows the distribution of $f_{\rm gas,merger}$ in three redshift bins in EAGLE. We find that the distributions are mostly bimodal, and we use this to define gas-rich ($f_{\rm gas,merger} \geq 0.5$) and gas-poor ($f_{\rm gas,merger} \leq 0.2$) mergers, as shown by the vertical dotted lines. From now on, we name these two subsamples as 'wet' and 'dry' mergers, respectively. At $0 \leq z \leq 3$, these two samples are made of 2677 and

1775 mergers, respectively, and have median $f_{\rm gas,merger}$ of 1.1 and 0.02, respectively. In the literature, 'dry' mergers usually refer to galaxies completely devoid of gas (e.g. Makino & Hut 1997; Naab, Jesseit & Burkert 2006a; Taranu, Dubinski & Yee 2013). However, the reason behind that definition was mostly technical: Mergers were studied with collisionless simulations. However, in reality galaxies are expected to have some gas, even in the regime of 'red and dead' passive galaxies, as shown by ATLAS^{3D} (Young et al. 2011; Serra et al. 2012). EAGLE allows us to define 'dry' mergers in a more realistic fashion, by simply imposing them to be gas-poor. When we dissect $f_{\rm gas,merger}$ into the contributions from the primary (the one with the highest stellar mass) and secondary galaxies, we find that at any redshift the total gas fraction is dominated by the primary galaxy. In EAGLE, we find a good correlation between $f_{\rm gas,merger}$ of the primary and the secondary galaxy, which is stronger at high redshift. This correlation is a consequence of the 'conformity' of the galaxy population (i.e. gas-rich galaxies tend to be surrounded by gas-rich galaxies; Kauffmann et al. 2013; Wang et al. 2015; Hearin et al. 2016).

We calculate radial j profiles as in Lagos et al. (2017), which is a measurement if a mass-weighted average $j_{\rm stars}$ within r (i.e. $\equiv |J(<r)|/M(<r)$). We will refer to these measurements as 'mean radial $j_{\rm stars}$ profiles'. Lagos et al. (2017) showed that $j_{\rm stars}(r_{50})$, calculated with all particles within the half-stellar mass radius r_{50}, converges in EAGLE at $M_{\rm stars} \gtrsim 10^{9.5}\,{\rm M}_\odot$, and thus, we limit our sample only to galaxies with stellar masses above that threshold. Schaller et al. (2015a) showed that the stellar mass radial profiles of galaxies in EAGLE are well converged to scales of at least ≈1.5 pkpc. Schaller et al. (2015b) analysed the effect of the hydrodynamic scheme on galaxy properties and concluded that those were minimal compared to the effect of the subgrid modelling, showing that any numerical effects affecting the AM of galaxies are much less important compared to how the baryon physics is modelled (see also Scannapieco et al. 2012 and Pakmor et al. 2016). We also tested the convergence of the $j_{\rm stars}$ profiles using higher resolution runs and find good convergence down to $\approx 0.5\, r_{50}$ (see Appendix A). Thus, we consider EAGLE to have an appropriate resolution to perform our study on the effect of mergers on $j_{\rm stars}$.

We calculate two angles determining how mergers are oriented: (i) $\theta_{\rm spin}$, the angle subtended between the $\boldsymbol{j}_{\rm stars}$(tot) vectors of the two galaxies that are about to merge, and (ii) $\theta_{\rm orb}$, the angle between $\boldsymbol{j}_{\rm stars}$(tot) of the primary galaxy and the orbital AM vector,

$$\theta_{\rm spin} = \arccos\left[\hat{j}^{\rm s}_{\rm stars}({\rm tot}) \cdot \hat{j}^{\rm p}_{\rm stars}({\rm tot})\right], \quad (2)$$

and

$$\theta_{\rm orb} = \arccos\left[\hat{j}_{\rm orbital} \cdot \hat{j}^{\rm p}_{\rm stars}({\rm tot})\right], \quad (3)$$

where $\boldsymbol{j}^{\rm s}_{\rm stars}$(tot) and $\boldsymbol{j}^{\rm p}_{\rm stars}$(tot) are the normalized $j_{\rm stars}$ vectors of the secondary and primary galaxies, respectively, and $\boldsymbol{j}_{\rm orbital} = \boldsymbol{r} \times \boldsymbol{v}$. Here, $\boldsymbol{r}$ and $\boldsymbol{v}$ are the position and velocity vectors of the secondary galaxy in the rest frame of the primary one, calculated in the last snapshot the two galaxies were identified as separate objects. Galaxy growth produced by gas accretion and star formation will be termed 'smooth accretion' during the rest of the paper.

The top and middle panels of Fig. 2 show the merger rate density of minor and major mergers in (primary) galaxies with $M_{\rm stars} > 10^{9.5}\,{\rm M}_\odot$ as a function of redshift, respectively, and split into wet and dry. The frequency of mergers is noisy due to the small volume of the simulation and the relatively high stellar mass threshold we are applying to our galaxy sample. The frequency of dry mergers increases from $z = 2.5$ down to $z = 1$ in both minor and major mergers, with an approximately constant

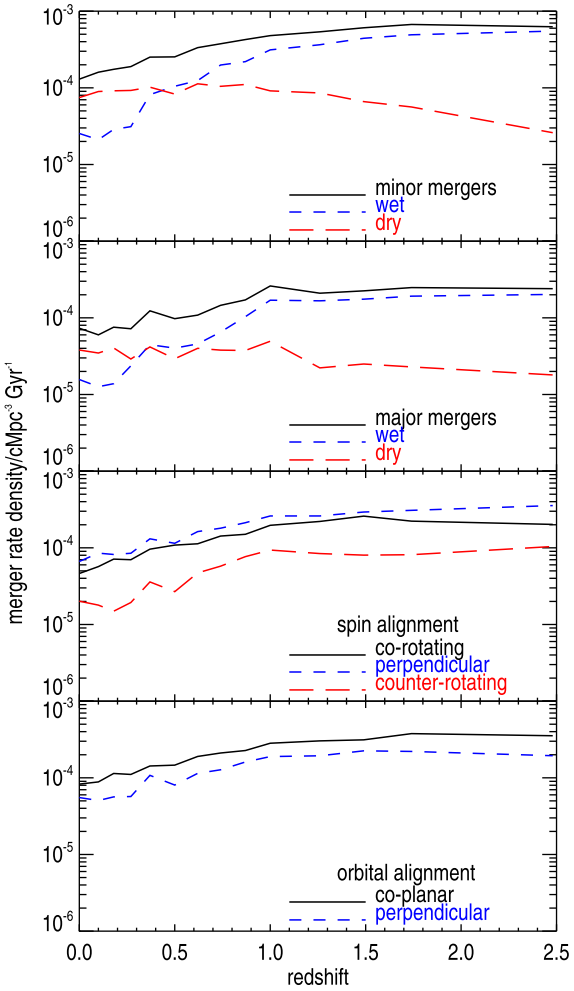

Figure 2. Merger rate density as a function of redshift in EAGLE. The top panel shows minor mergers and the subsamples of wet and dry minor mergers, as labelled. The middle panel is the same but for major mergers, while the bottom panels show mergers split into spin (i.e. corotating, perpendicular and counter-rotating) and orbital (i.e. coplanar and perpendicular) alignments, respectively.

frequency at $z < 1$. The frequency of wet mergers instead decreases steadily towards $z = 0$. This is driven by EAGLE galaxies having $f_{\rm gas,merger}$ that decrease with time (Lagos et al. 2015, 2016). The bottom panels of Fig. 2 show the frequency of mergers split by their spin orientation and orbital alignment. In the case of spin alignments, we define corotating, perpendicular and counter-rotating mergers as those with $\cos(\theta_{\rm spin}) > 0.7$ (angles between 0° and 45°), $-0.15 < \cos(\theta_{\rm spin}) < 0.15$ (angles between 81°and99°) and $\cos(\theta_{\rm spin}) < -0.7$ (angles between 135°and180°), respectively. Randomly oriented mergers in three dimensions would imply a uniform distribution in $\cos(\theta_{\rm spin})$; hence, the number of mergers in these equal ranges (0.3 in $\cos(\theta_{\rm spin})$) directly show their relative frequency. We find in EAGLE that perpendicular mergers are ≈1.3 times more common than corotating mergers, but counter-rotating mergers are ≈3.4 and ≈2.6 times less common than perpendicular and corotating mergers, respectively. In the case of orbital alignments, we define coplanar mergers as those with $|\cos(\theta_{\rm orb})| \geq 0.7$, while perpendicular mergers have $|\cos(\theta_{\rm orb})| \leq 0.3$. We find that coplanar mergers are ≈1.5 more frequent than perpendicular ones. The

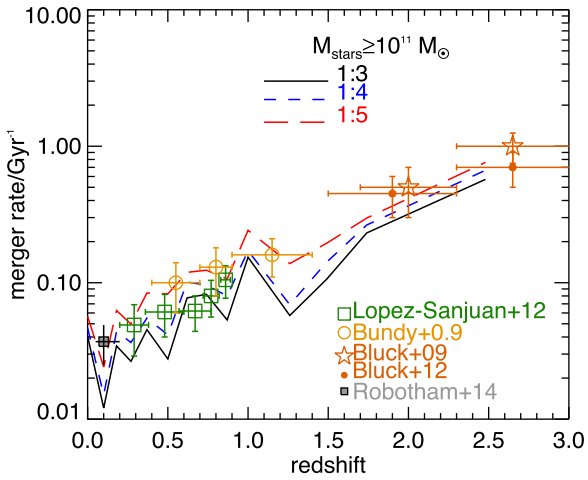

Figure 3. Merger rate in galaxies with $M_{\rm stars} \geq 10^{11}\,{\rm M}_{\odot}$ in EAGLE as a function of redshift. We show merger ratios $\geq$1 : 3 (solid line), $\geq$1 : 4 (short-dashed line) and $\geq$1 : 5 (long-dashed line). We also show the observational measurements of Bundy et al. (2009), Bluck et al. (2009), López-Sanjuan et al. (2012), Bluck et al. (2012) and Robotham et al. (2014). Most of these observational works assume major mergers are those with stellar mass ratios $\geq$1 : 4. EAGLE predicts major merger rates of massive galaxies that are in excellent agreement with the observations in the entire redshift range where measurements are available.

trends we see here are consistent with those presented by Welker et al. (2015) using the HORIZON-AGN simulation. Welker et al. (2015) showed that satellite galaxies on a decaying orbit towards the central galaxy tend to align with the galactic plane of the central in a way that, by the time they merge, they are most likely to come in an orbit aligned with the galactic plane of the primary. Welker et al. (2015) also found that mergers taking place in filaments are more likely to be of galaxies with $\cos(\theta_{\rm spin}) \approx 0$ if the primary galaxy is a passive, spheroidal galaxy, while corotation is expected if the primary galaxy is a spiral, star-forming galaxy. The frequencies we report in the bottom panels of Fig. 2 are consistent with this picture.

Fig. 3 compares the major merger rate of EAGLE galaxies with $M_{\rm stars} \geq 10^{11}\,{\rm M}_{\odot}$ at different redshifts against a compilation of observations. Here, we employ three different stellar mass ratios to define major mergers: $\geq$1 : 5, $\geq$1 : 4 and $\geq$1 : 3, to show the systematic variations produced by this definition. The observations shown in Fig. 3 correspond to measurements coming from the characterization of pair frequency (Bluck et al. 2009; Bundy et al. 2009; López-Sanjuan et al. 2012; Robotham et al. 2014), and from the identification of galaxies with disturbed morphologies (Bluck et al. 2012). Both set of measurements agree remarkably well. We find that the major merger rate of massive galaxies is in excellent agreement with the observations. For our purpose, this means that the effect of galaxy mergers on the AM of galaxies is not going to be over(under)represented.

3 THE EFFECT OF MERGERS ON THE STELLAR SPECIFIC AM OF GALAXIES THROUGHOUT COSMIC TIME

In Section 3.1, we present an analysis of the accumulated effect of mergers by studying the galaxy population at $z = 0$. In Section 3.2, we analyse the effect of mergers by comparing measurements of galaxy properties before and after the mergers, and how these depend on the nature of the merger. In Section 3.3, we analyse the radial rearrangement of $j_{\rm stars}$ as a result of mergers.

3.1 The net effect of galaxy mergers seen at $z = 0$

The top-left panel of Fig. 4 shows how the galaxy merger rate changes with the position of galaxies in the $j_{\rm stars}(r_{50})$–$M_{\rm stars}$ plane. We define the average merger rate of individual galaxies as the number of mergers divided by the stellar-mass-weighted age. Here, we do not distinguish recent from past mergers, but just count their occurrence. We colour only those bins in which at least 50 per cent of the galaxies have undergone mergers during their lifetimes. This is why below $M_{\rm stars} \approx 10^{10}\,{\rm M}_{\odot}$ there are very few coloured bins. At $10^{10}\,{\rm M}_{\odot} \lesssim M_{\rm stars} \lesssim 10^{10.5}\,{\rm M}_{\odot}$ mostly galaxies with low spins have a significant contribution from mergers. These galaxies are hosted by haloes that are on average 20 per cent more massive than those of galaxies of the same stellar mass but that never had mergers. At $M_{\rm stars} \gtrsim 10^{10.5}\,{\rm M}_{\odot}$ the vast majority of galaxies had at least one merger by $z = 0$. The merger rate increases with increasing mass (best power-law fit is $\propto M_{\rm stars}^{0.1}$), and no clear correlation is seen with $j_{\rm stars}(r_{50})$ at fixed stellar mass.

In the top-middle and right-hand panels of Fig. 4, we calculate the fraction of the mergers shown in the left-hand panel that were minor and major, respectively. We also performed power-law best fits to the relationship between the merger fraction and $M_{\rm stars}$ and $j_{\rm stars}(r_{50})$ to quantify the trends. The best-fitting power-law indices are shown in each panel of Fig. 4.

The fraction of major and minor mergers weakly increase and decrease, respectively, with increasing stellar mass (see the power-law indices in Fig. 4). We also see a slightly stronger trend with $j_{\rm stars}(r_{50})$: At fixed stellar mass, the frequency of major and minor mergers decrease and increase, respectively, with increasing $j_{\rm stars}(r_{50})$. The directions in which the frequency of mergers increase are shown as arrows in Fig. 4.

In the bottom panels of Fig. 4, we split the mergers into dry and wet, following the definition of Fig. 1. We find stronger trends with both $M_{\rm stars}$ and $j_{\rm stars}(r_{50})$. For dry mergers, we find an increase in their frequency with increasing stellar mass, and we identify a significant gradient of an increasing fraction of dry mergers with decreasing $j_{\rm stars}(r_{50})$ at fixed stellar mass (see the power-law indices in the bottom panel of Fig. 4). For wet mergers, we find that their fraction increases with decreasing stellar mass and increasing $j_{\rm stars}(r_{50})$. The latter though is a very weak trend. Fig. 4 indicates that the gas fraction involved in the merger is more important than the mass ratio for the current $j_{\rm stars}(r_{50})$ of galaxies. We examine the same plots for $j_{\rm stars}$ measured within $5\,r_{50}$ (used to encompass the entire galaxy) and find the same trends (not shown here). These results suggest that galaxy mergers can have a devastating effect on the specific AM of galaxies, but with the exact effect strongly depending on the nature of the merger.

Lagos et al. (2017) found that the positions of galaxies in the $j_{\rm stars}(r_{50})$–$M_{\rm stars}$ plane are strongly correlated with a galaxy's gas fraction, stellar age, stellar concentration, optical colour and V/σ, all of which are usually used to distinguish early- and late-type galaxies. In Fig. 5, we explicitly show how the morphology of galaxies changes in this plane. Here, we randomly selected galaxies in 10 bins of $\log_{10}(j_{\rm stars}(r_{50}))$ and 8 bins of $\log_{10}(M_{\rm stars})$ in the ranges $10^{0.5}-10^{3}$ pkpc km s^{-1} and $10^{10}-10^{12}\,{\rm M}_{\odot}$, respectively, and extract their synthetic optical images from the EAGLE data base. These images are face-on views and are 60 pkpc on a side. This figure shows that at fixed $M_{\rm stars}$, galaxies go from being red spheroidals at low $j_{\rm stars}(r_{50})$ to being grand-design spirals at high $j_{\rm stars}(r_{50})$ in the

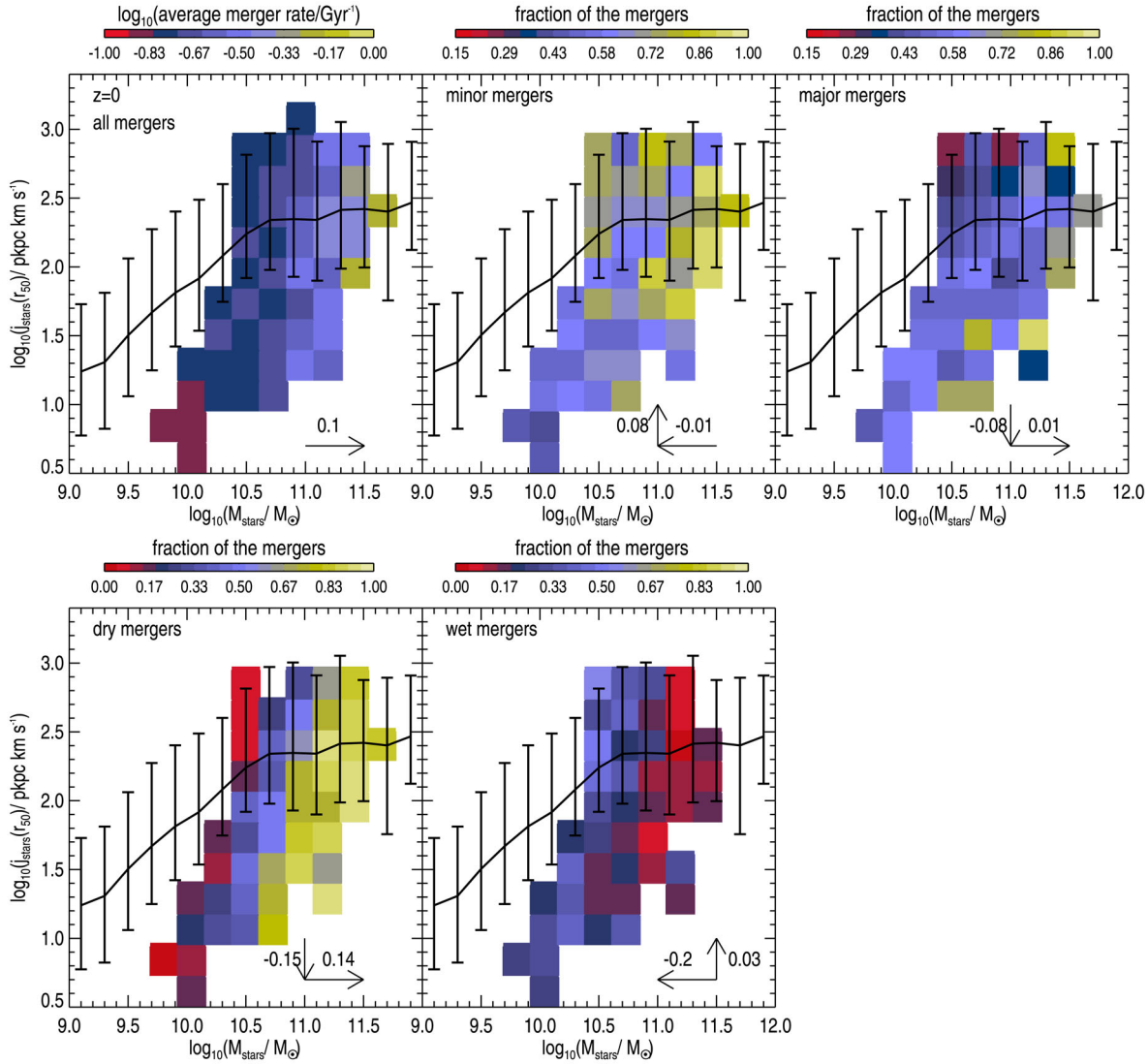

Figure 4. Top panels:The specific AM of the stars measured with all the particles within the half-mass radius of the stellar component as a function of stellar mass at $z = 0$ for galaxies with $M_{\rm stellar} > 10^9\,{\rm M}_\odot$ in EAGLE. The lines with error bars show the median and the 16th–84th percentile ranges. In the left-hand panel, we colour bins (with $\geq$5 galaxies) in which more than 50 per cent of the galaxies have suffered mergers, by the average merger rate per galaxy they had during their lifetimes. In the middle and right-hand panels, we coloured those same bins by the fraction of the mergers that were minor and major, respectively. By construction, the fractions of the middle and right-hand panels in each two-dimensional bin add up to 1. Bottom panels: As in the top-middle and right-hand panels, but for the fraction of the mergers that were dry and wet, respectively. The arrows in each panel indicate the directions in which the frequency of the respective merger type increases and the number next to the arrows show the best-fitting power-law index for the relations: average merger rate $\propto M^\alpha$, merger fraction $\propto M^\alpha$ and merger fraction $\propto j^\alpha$.

stellar mass range $10^{10}\,{\rm M}_\odot \lesssim {\rm M}_{\rm stars} \lesssim 10^{11}\,{\rm M}_\odot$. At higher stellar masses, galaxies with high $j_{\rm stars}(r_{50})$ appear more like defunct spirals, with little star formation and aging discs. If we follow the median $j_{\rm stars}(r_{50})$, one sees that galaxies go from being preferentially spiral/disc-dominated at $M_{\rm stars} \approx 10^{10}\,{\rm M}_\odot$ to spheroids at $M_{\rm stars} \gtrsim 10^{11.5}\,{\rm M}_\odot$. Given the strong correlation between the positions of galaxies in the $j_{\rm stars}(r_{50})$–$M_{\rm stars}$ plane with the frequency of wet/dry mergers, and with the morphologies of galaxies, one would expect morphologies to be connected to wet/dry mergers. Rodriguez-Gomez et al. (2017) showed that the morphologies of galaxies are connected with the merger history in the Illustris simulation, but they could only determine a clear correlation in massive galaxies, $M_{\rm star} \geq 10^{11}\,{\rm M}_\odot$, due to predominance of dry mergers and *exsitu* formation of the stars. Our results in EAGLE suggest that the morphology of galaxies, as well as their $j_{\rm stars}$, sensitively depend on the type of the merger.

To corroborate this relation, in Fig. 6 we show the 3D Sérsic index (measured from the 3D stellar mass distributions) and the kinematic bulge-to-total, B/T, ratio[1] as a function of stellar mass for galaxies at $z = 0$ that have not suffered mergers, and had at least one dry or wet merger. This figure shows that no-merger galaxies have much lower Sérsic indices and B/T ratios than galaxies that

[1] ${\rm B/T} \equiv 1 - \kappa_{\rm co}$, where $\kappa_{\rm co}$ is the ratio of kinetic energy invested in ordered rotation calculated using only star particles that follow the direction of rotation of the galaxy (see Correa et al. 2017 for more details). We also analysed the Abadi et al. (2003) and Sales et al. (2010) definitions of kinetic B/T and found the same trends as in the bottom panel of Fig. 6.

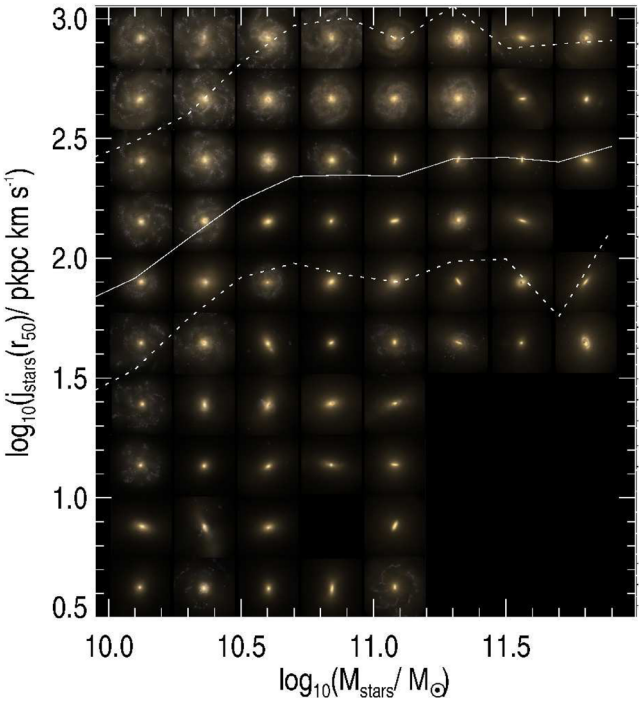

Figure 5. Visualizationof the optical morphology of galaxies in the $j_{stars}(r_{50})$–M_{stars} plane at $z = 0$. We randomly select galaxies in 10 bins of $\log_{10}(j_{stars}(r_{50}))$ and 8 bins of $\log_{10}(M_{stars})$ in the range $10^{0.5}-10^{3}$ pkpc km s^{-1} and $10^{10}-10^{12}$ M$_\odot$, respectively, and show here their synthetic *g*, *r*, *i* face-on optical images. Only bins with ≥3 galaxies are shown here. These images are 60 pkpc on a side are publicly available from the EAGLE data base (McAlpine et al. 2016). The solid and dotted lines show the median and the 16th–84th percentile range.

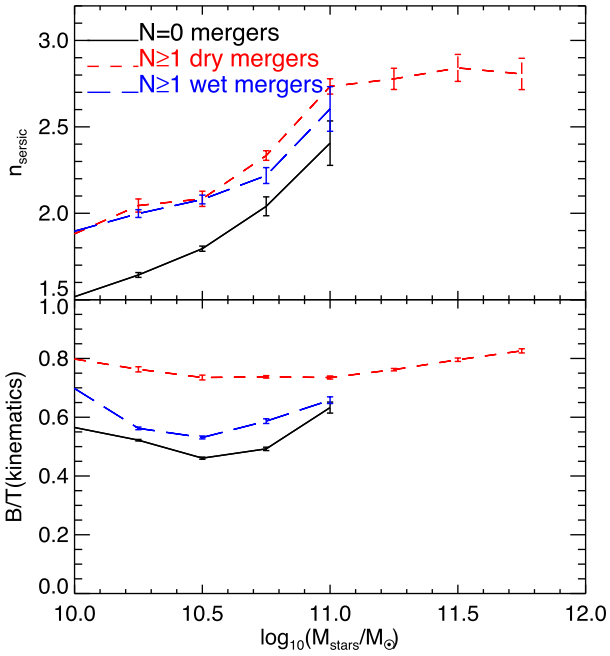

Figure 6. Sérsic index (top) and kinematic bulge-to-total ratio (bottom) as a function of stellar mass for galaxies at $z = 0$. We show galaxies with $M_{stellar} \geq 10^{10}$ M$_\odot$, which is where galaxy mergers become common (see the top-left panel of Fig. 4). Lines with error bars show the median and 1σ error on the median for galaxies that have not had mergers, and those that had at least one dry or wet merger, as labelled in the top panel, by $z = 0$. This figure shows that galaxies that suffered dry mergers have the highest Sérsic indices and B/T ratios.

had mergers. Galaxies that had dry mergers also have the highest Sérsic indices and B/T ratios, confirming the connection we see between the visual morphologies of Fig. 5 and the frequency of dry mergers in Fig. 4. Galaxies that had wet mergers have Sérsic indices and B/T ratios lower than the dry merger remnants, but higher than the no-merger galaxies. This is consistent with the findings discussed in Section 3.3.1 of the central stellar concentration in galaxies increasing during wet mergers. We explore the effect of mergers on $j_{stars}(r_{50})$ further in Section 3.2.

We now examine the mean radial j_{stars} profiles of galaxies at $z = 0$ in Fig. 7 in a narrow range of stellar mass, $10^{10.5}$ M$_\odot \lesssim$ M$_{stars} \lesssim 10^{11}$ M$_\odot$. In the same figure, we also show the cumulative radial profile of M_{stars}. In the top panel, we show how different the radial j_{stars} profiles are in galaxies that suffered different numbers of mergers, without yet distinguishing the type of merger. Increasing the frequency of mergers has the effect of flattening the radial j_{stars} profile, in a way that galaxies that went through a higher number of mergers have a deficit of j_{stars} at $0.5\,r_{50} \lesssim r \lesssim 10\,r_{50}$ as large as ≈0.3 dex compared to their counterparts of the same mass but that did not go through mergers. At sufficiently large radii, j_{stars} converges so that galaxies with different number of mergers have a similar j_{stars}(tot). This suggests that the most important effect of mergers is in the radial structure of j_{stars} rather than the total j_{stars}. The stellar mass cumulative profile of galaxies is also shallower when the frequency of mergers increases, which means that a larger fraction of the stellar mass is locked up in the outskirts of galaxies. Although there is a small tendency for galaxies that went through more mergers to have a larger r_{50}, the trends here are not affected by this, as the differences in the radial profiles are very similar even when we do not normalize the *x*-axis by r_{50}. By splitting mergers into minor and major (second and third panels of Fig. 7), we find that galaxies that had one major merger can have a deficit in j_{stars} similar to those that had two minor mergers, and increasing the frequency of major mergers does not seem to have the cumulative effect that is seen for minor mergers. In our sample, EAGLE galaxies that had major mergers can have minor mergers too, but for the sample of minor mergers, we remove all galaxies that had at least one major merger.

We then analyse mergers split into dry and wet in the bottom panels of Fig. 7 and find that *dry mergers have a catastrophic* effect on j_{stars} from the galaxy's centre out to ≈20 r_{50}. The deficit of j_{stars} compared to galaxies without a merger is as large as ≈0.5 dex. Also note that the stellar mass cumulative profile is much shallower for galaxies that went through a dry merger. In the case of wet mergers, we see the exact opposite. Very little difference is found between galaxies that did not suffer a merger and those that suffered one, two or more wet mergers. This reinforces the conclusion that to j_{stars} of a galaxy, what matters most is whether the merger is dry or wet. We will show in Fig. 11 that this is also true when we study j_{stars} before and after the merger. Note that in the case of dry mergers, we still see that the mean radial j_{stars} profile converges at sufficiently large radii to a j_{stars}(tot) that does not strongly depend on the merging history of galaxies.

3.1.1 *The galaxy/halo specific AM connection*

We compare j_{stars} of the galaxies with the specific AM of their dark matter haloes in the top panel of Fig. 8. We find that galaxies that went through at least one dry merger on average have a j_{stars}(tot) that is five times smaller than that of their halo, while galaxies that

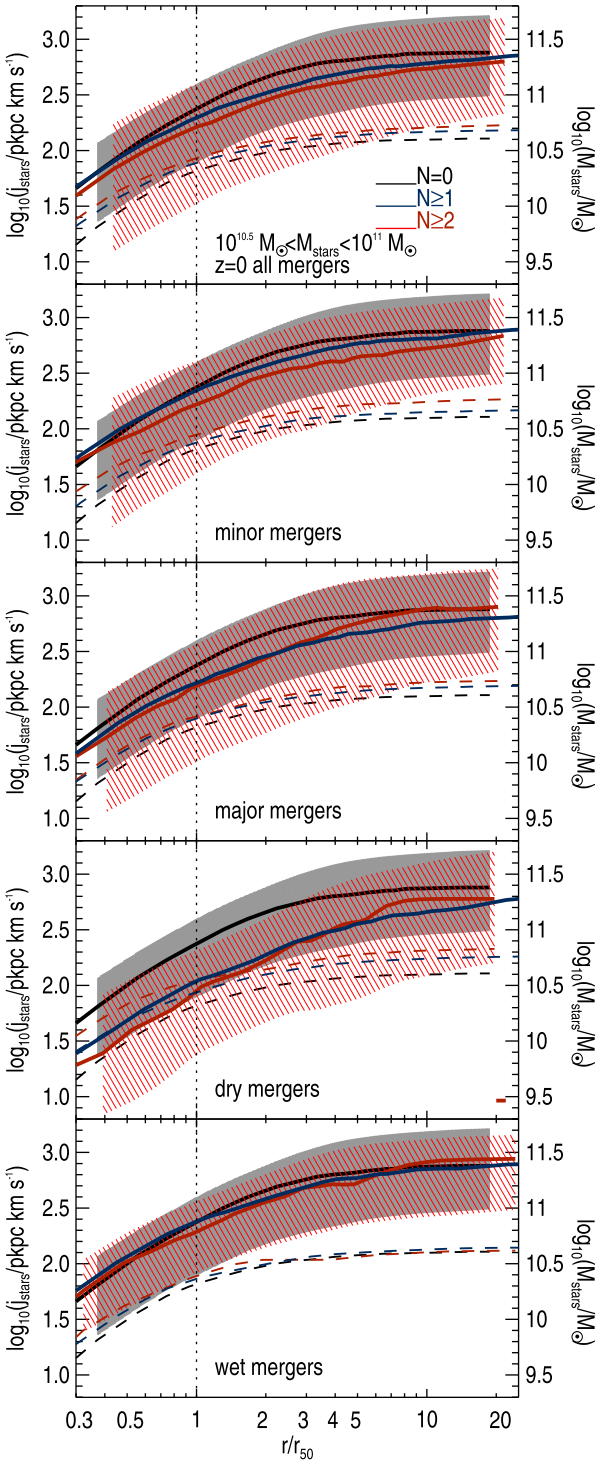

Figure 7. Top panel: $j_{\rm stars}$ (solid lines) and $M_{\rm stars}$ (dashed lines) measured within r as a function of r in units of r_{50} for galaxies at $z = 0$ with total stellar masses in the range $10^{10.5}\,{\rm M}_\odot - 10^{11}\,{\rm M}_\odot$ that have gone through different numbers of galaxy mergers, as labelled. Lines show the median of the $j_{\rm stars}$ profiles of galaxies, while the shaded regions show the 16th–84th percentile range, plotted only for $N_{\rm mergers} = 0, \geq 2$, for clarity. The scale of $j_{\rm stars}$ and $M_{\rm stars}$ are marked in the left and right axis, respectively. Other panels: As in the top panel, but distinguishing between minor, major, dry and wet mergers, as labelled. This figure shows that galaxy mergers generally lead to a deficit of $j_{\rm stars}$ at $r \lesssim 10\,r_{50}$, with dry mergers causing pronounced deficits of ≈0.5 dex. At sufficiently large radii, $j_{\rm stars}$ converges to a value set by the dark matter halo.

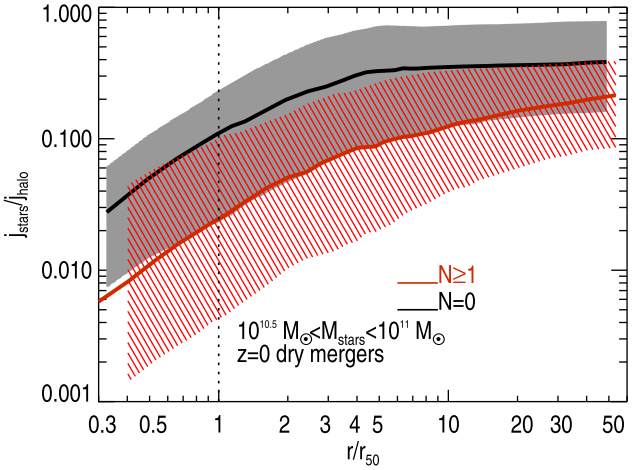

Figure 8. As Fig. 7, but for the subsample of central galaxies at $z = 0$ that have not suffered a merger (black solid line) and those that went through at least one dry merger (red solid line), and that have stellar masses in the range $10^{10.5}\,{\rm M}_\odot - 10^{11}\,{\rm M}_\odot$. Here, we show $j_{\rm stars}$ in units of the specific AM of the dark matter halo, $j_{\rm halo}$, calculated with all dark matter particles within the virial radius. Galaxies that did not have a merger typically have $j_{\rm stars}$ increasing from ≈0.1 at r_{50} to ≈0.4 $j_{\rm halo}$ at $10\,r_{50}$, while galaxies that had at least one dry merger go from ≈0.02 to ≈0.2 $j_{\rm halo}$ in the same radii range, on average.

did not go through a merger typically retain ≈40–50 per cent of their halo j. The latter result agrees very well with the prediction by Stevens et al. (2016) for spiral galaxies. With a semi-analytic model, those authors evolved the one-dimensional structure of discs in a series of annuli of fixed j. They assumed that when gas cooled or accreted on to a galaxy, it carried the same total j of the halo *at that time* in both magnitude and direction, and that it was distributed exponentially. Stars were formed in annuli that were Toomre unstable or had sufficient H_2. At $z = 0$, they found spiral galaxies (which had not suffered dry mergers) had $j_{\rm stars}/j_{\rm halo} = 0.4 \pm 0.29$, independent of galaxy mass (see their fig. 13). Despite the completely different methodology, this aligns almost perfectly with the result of EAGLE galaxies that have not participated in a dry merger.

Fall (1983) suggested that spiral galaxies need to have a $j_{\rm stars}$ close to that of their halo (within ≈80 per cent according to Fall & Romanowsky 2013), while ellipticals had to lose 90 per cent of their j, postulating a fundamental difference between the two galaxy populations. The conclusions reached by these authors were biased by the available observations, that in the best case went out to $\approx 10\,r_{50}$. According to EAGLE, early-type galaxies only reach ≈0.1 of the expected halo j at $r \approx 10 r_{50}$, on average. EAGLE shows that $j_{\rm stars}$ continues to rise out to much larger radii due to the effect of adding halo stars. EAGLE predicts that this difference shrinks at larger radii, although still not converging to a fraction of $j_{\rm halo}$ as high as galaxies with no mergers in their lifetime. Early simulations of mergers predicted that dynamical friction could redistribute AM from the inner to the outer regions (e.g. Barnes & Efstathiou 1987; Navarro & White 1994; Heyl et al. 1996). From those simulations, one would expect a net weak conservation of j. Our findings with EAGLE show a significant disparity between the stellar and the halo j, but that is not as large as that suggested by some of the idealized models (Romanowsky & Fall 2012).

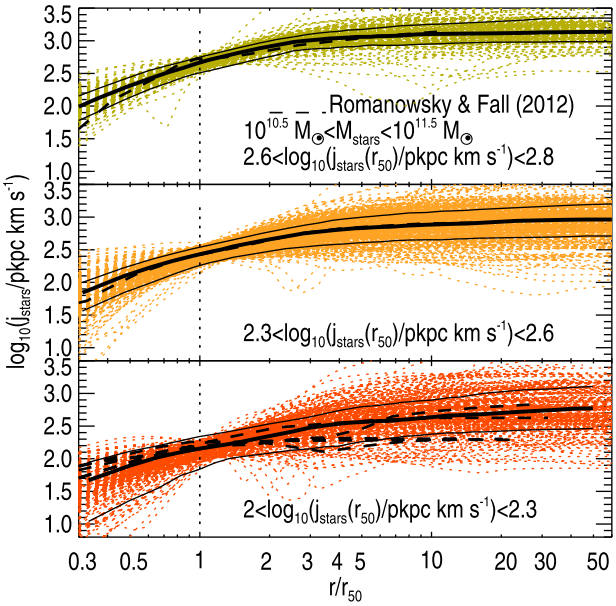

Figure 9. Mean radial $j_{\rm stars}$ profiles for galaxies in EAGLE at $z = 0$ and with stellar masses in the range $10^{10.5}\,{\rm M}_{\odot}-10^{11.5}\,{\rm M}_{\odot}$ in three bins of $j_{\rm stars}(r_{50})$, as labelled in each panel. The dotted lines show all galaxies in that range, while the thick and thin solid lines show the median, and the 16th and 84th percentile ranges, respectively. We show observations of early-type galaxies from Romanowsky & Fall (2012) as dashed lines. Their sampled galaxies have stellar masses in the range we selected here, and we show each galaxy in their corresponding bin of $j_{\rm stars}(r_{50})$. Here, we only show the median measurement, but error bars around those measurements can be as large as ≈0.5 dex, particularly at $r \gtrsim 3\,r_{50}$.

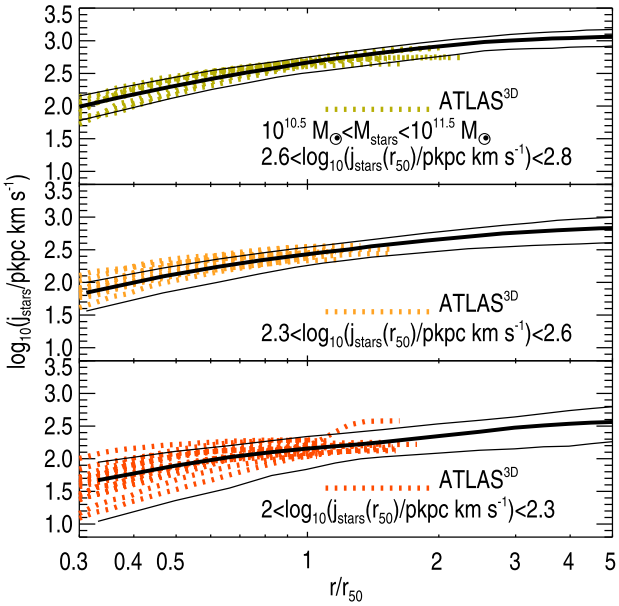

Figure 10. Mean radial $j_{\rm stars}$ profile for the same EAGLE galaxies of Fig. 9. For the simulated galaxies, we show the median and the 16th and 84th percentile ranges. Individual dotted lines show ATLAS$^{\rm 3D}$ galaxies that have stellar masses in the range $10^{10.5}\,{\rm M}_{\odot}-10^{11.5}\,{\rm M}_{\odot}$ and have $j_{\rm stars}(r_{50})$ in the ranges shown in each panel. The agreement between EAGLE and the observations is excellent.

3.1.2 *Comparison with observations of early-type galaxies*

We compare EAGLE galaxies of low $j_{\rm stars}$ with the observations of Romanowsky & Fall (2012) in Fig. 9. Romanowsky & Fall (2012) presented mean radial $j_{\rm stars}$ profiles for seven ellipticals and S0 galaxies in the stellar mass range of $10^{10.5}\,{\rm M}_{\odot} \lesssim {\rm M}_{\rm stars} \lesssim 10^{11.5}\,{\rm M}_{\odot}$. We took these seven galaxies and separated them into three bins of $\log_{10}(j_{\rm stars}(r_{50})/{\rm pkpc\,km\,s^{-1}})$, 2–2.3, 2.4–2.6 and 2.6–2.8, in which EAGLE would correspond to galaxies below, close to and above the median $j_{\rm stars}(r_{50})$ at that stellar mass, and compare them with EAGLE in Fig. 9. In EAGLE, most galaxies of such stellar mass are expected to be of early type (see Figs 5 and 6). We find that at low $j_{\rm stars}$ (bottom panel of Fig. 9) the scatter in the mean radial profiles becomes increasingly larger compared to galaxies of higher $j_{\rm stars}$, and galaxies with flat mean $j_{\rm stars}$ profiles become more common. The diversity of mean radial $j_{\rm stars}$ profiles observed by Romanowsky & Fall (2012) is well captured by EAGLE, even in the cases where $j_{\rm stars}$ ceases to increase at $r \gtrsim 3\,r_{50}$.

With the aim of testing EAGLE with a larger number of galaxies, we extracted mean radial $j_{\rm stars}$ profiles for every ATLAS$^{\rm 3D}$ galaxy (Cappellari et al. 2011), following the procedure described in Lagos et al. (2017). These profiles sample up to ≈2 r_{50} in the best cases, but they inform us of the shape of the radial $j_{\rm stars}$ profile in the inner regions of galaxies. Fig. 10 shows the comparison between EAGLE and ATLAS$^{\rm 3D}$ in the same stellar mass and $j_{\rm stars}(r_{50})$ ranges of Fig. 9. From top to bottom, each panel shows 8, 10 and 15 ATLAS$^{\rm 3D}$ galaxies, respectively. The agreement with the observations is excellent. ATLAS$^{\rm 3D}$ galaxies show a larger scatter in the radial $j_{\rm stars}$ profiles with decreasing galaxy spins, which is very similar to the trend seen in EAGLE. This gives us confidence that the simulation not only reproduces the average j-mass relation, as shown by Lagos et al. (2017), but also the radial profiles of galaxies, where observations exists. The number of galaxies in the Universe in which this comparison can be done is still very sparse, but the advent of IFU instruments (e.g. SAMI, MaNGA, MUSE) is likely to change this.

3.2 $j_{\rm stars}$ before and after galaxy mergers

We analyse how much $j_{\rm stars}(r_{50})$ changes between two consecutive snapshots for galaxies with $M_{\rm stars} \geq 10^{9.5}\,{\rm M}_{\odot}$ and in the redshift range $0 \leq z \leq 2.5$, separating galaxies into those that had and did not have a merger, and splitting mergers into different types: minor/major, wet/dry and with different spin alignments and orbital parameters. This is shown in the top panel of Fig. 11 (the equivalent for $j_{\rm stars}(5r_{50})$ is shown in Fig. C1). The bottom panel of Fig. 11 shows the fraction of galaxies displaying an increase in $j_{\rm stars}(r_{50})$ for the same cases analysed in the top panel. The first three data points compare the change in $j_{\rm stars}(r_{50})$ due to smooth accretion and a minor or major merger. In the latter case, star formation and gas accretion may continue, and thus, we cannot fully separate this effect from the merger. Galaxies that did not suffer mergers on average increase their $j_{\rm stars}(r_{50})$ by ≈15 per cent in between snapshots, and are likely to undergo an important increase in $j_{\rm stars}(r_{50})$ (i.e. ≈35 per cent of the galaxies at least double their $j_{\rm stars}(r_{50})$ in a snapshot). On the contrary, galaxy mergers are more likely not to change or reduce their $j_{\rm stars}(r_{50})$, depending on whether they are minor or major mergers, respectively. From the bottom panel of Fig. 11, one sees that smooth accretion increases $j_{\rm stars}(r_{50})$ ≈60 per cent of the time, while minor and major mergers do this only in ≈54 per cent and ≈43 per cent of the cases, respectively.

Fig. 11 also splits mergers into several subsamples to pin down the circumstances in which $j_{\rm stars}$ change the most. We first take all of the minor and major mergers and split them into dry and wet (shown from the 4th to the 7th symbols and bars in Fig. 11). We find that

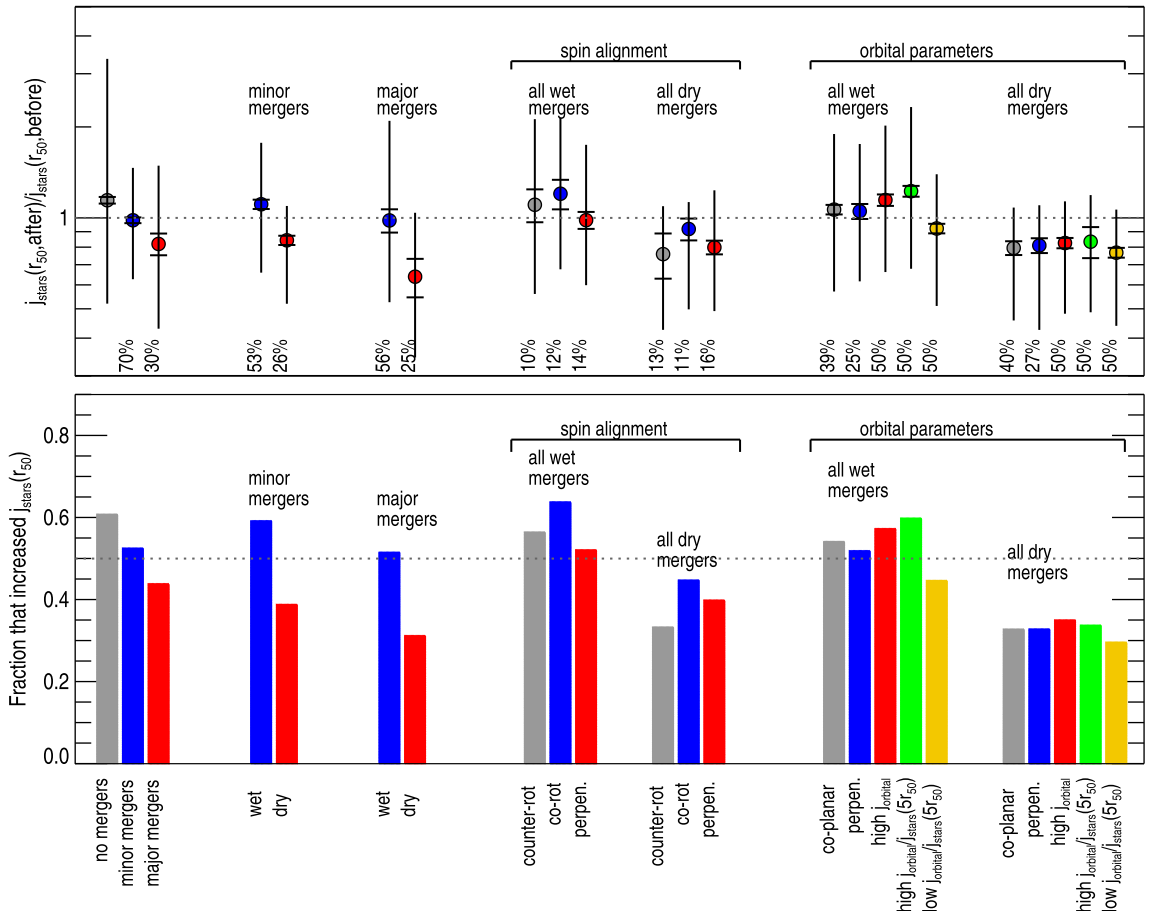

Figure 11. Top panel:the ratio of $j_{stars}(r_{50})$ in a galaxy between two consecutive snapshots. We separate galaxies into those that had no mergers, and those that went through a minor or a major merger (first three symbols); galaxies that went through a minor or major merger, separated into wet and dry (subsequent four symbols); galaxies that went through wet and dry mergers separated into three samples of spin alignment (counter-rotating, corotating and perpendicular, as defined in Section 2; subsequent six symbols), and separated into five orbital parameter samples (coplanar and perpendicular mergers, and mergers with high orbital AM, and high/low orbital-to-central galaxy AM; subsequent 10 symbols), as labelled in the *x*-axis. The symbols show the medians, while the small and large error bars show the statistical uncertainty on the median (from bootstrap resampling) and the 25th−75th percentile ranges, respectively. The dotted line shows no change in $j_{stars}(r_{50})$. At the bottom of the panel, we show the percentage of the mergers that are included in each subsample. Bottom panel: fraction of galaxies that display an increase in their $j_{stars}(r_{50})$ in the same cases shown for the same selections of the top panel. For reference, the dotted line shows a fraction of 0.5. We find that on average galaxy mergers have a negative effect on $j_{stars}(r_{50})$, as a smaller fraction leads to an increase in $j_{stars}(r_{50})$ compared to smooth accretion. However, the nature of the merger has a large effect on the outcome: wet, corotating mergers tend to increase $j_{stars}(r_{50})$, while dry, counter-rotating mergers have the most negative effect on $j_{stars}(r_{50})$.

wet minor mergers produce a similar increase of $j_{stars}(r_{50})$ to smooth accretion, with a smaller percentage of galaxies going through a major increase in $j_{stars}(r_{50})$ (≈20 per cent of wet minor mergers produce an increase of a factor of $\gtrsim$2). Dry minor mergers, on the other hand, display a strong preference for decreasing $j_{stars}(r_{50})$. For major mergers, the trends are similar but with a larger difference between dry and wet mergers. Dry major mergers reduce $j_{stars}(r_{50})$ in ≈75 per cent of the cases, which shows that this is one of the most catastrophic forms of mergers for the AM budget of galaxies. Note that in EAGLE *the gas fraction of the merger is more important than the mass ratio*. We calculate the Kolmogorov–Smirnov (KS) *p*-value between dry and wet mergers for the cases of minor and major mergers and find that there is negligible probability, $<10^{-15}$, that they are drawn from the same population.

So far, we have stacked all of the galaxy mergers that take place in galaxies with $M_{stars} \geq 10^{9.5}$ M$_\odot$ and in the redshift range $0 \leq z \leq 2.5$. This may introduce significant biases due to the time interval between outputs of the simulation (different snapshots cover different time-scales), and also due to galaxies having very different sizes at different cosmic epochs. In Appendix C, we show that the bias introduced by studying mergers at different cosmic epochs and taking place in galaxies of different stellar masses is minimal, and that the difference seen here between minor/major, wet/dry mergers is of the same magnitude in subsamples of different redshifts and stellar masses. From here on, we analyse galaxy mergers together, regardless the cosmic epoch and the stellar mass of the galaxy in which they occur, unless otherwise stated.

Given the importance of wet/dry mergers over minor/major mergers, we explore the effect of spin alignments and orbital parameters in the subsamples of dry and wet mergers in the right part of Fig. 11. We first measure the effect of corotating ($\cos(\theta_{spin}) > 0.7$), perpendicular ($-0.15 < \cos(\theta_{spin}) < 0.15$) and counter-rotating ($\cos(\theta_{spin}) < -0.7$) mergers (middle symbols and bars in Fig. 11). We find that wet mergers between corotating galaxies lead to a larger and more frequent increase of $j_{stars}(r_{50})$, while perpendicular wet mergers tend to produce little changes in $j_{stars}(r_{50})$.

64 per cent of the corotating wet minor mergers increase $j_{\rm stars}(r_{50})$, a frequency that is even higher than smooth accretion. The effect of counter-rotating mergers is in between the corotating and perpendicular mergers. Perpendicular mergers are the most common configuration in EAGLE (see Fig. 2) and that is why the bars for wet minor and major mergers are skewed towards the results of perpendicular rather than corotating mergers. For dry mergers, we find the same trend: Corotating mergers tend to be less damaging than perpendicular or counter-rotating mergers for $j_{\rm stars}(r_{50})$.

In the rightmost part of Fig. 11, we analyse the effect of the orbital parameters. Particularly, we analyse coplanar and perpendicular mergers, the subsample with high $j_{\rm orbital}$ (i.e. higher than the median) and with high and low $j_{\rm orbital}/j_{\rm stars}(5r_{50})$ (above and below the median, respectively). Section 2.1 presents the definition of $j_{\rm orbital}$, and here, we compare $j_{\rm orbital}$ to $j_{\rm stars}(5r_{50})$ of the primary galaxy prior to the merger. $j_{\rm stars}(5r_{50})$ is a good measurement of the galaxy's total $j_{\rm stars}$ (see Fig. 7). We do not find a strong effect on the orientation of the mergers on $j_{\rm stars}(5r_{50})$, as both the distributions of the coplanar and perpendicular mergers are statistically indistinguishable (the KS p-value is 0.56). When comparing mergers of high and low $j_{\rm orbital}$, however, we find a significant difference (with a KS p-value of 10^{-5}) in which mergers with high $j_{\rm orbital}$ preferentially result in an increase in $j_{\rm stars}(5r_{50})$ of ≈15 per cent. The largest systematic is found when we separate wet mergers by their $j_{\rm orbital}/j_{\rm stars}(5r_{50})$ (the p-value comparing the two subsamples of high/low $j_{\rm orbital}/j_{\rm stars}(5r_{50})$ is 10^{-24}). High values of $j_{\rm orbital}/j_{\rm stars}(5r_{50})$ efficiently spin up the galaxy, increasing $j_{\rm stars}(r_{50})$ by ≈22 per cent on average, in 60 per cent of the cases. This suggests that galaxies spin-up because part of the orbital AM is transferred to the remnant galaxy. We study the subsample of wet, corotating ($\cos(\theta_{\rm spin}) > 0.7$) and high $j_{\rm orbital}/j_{\rm stars}(5r_{50})$ mergers, and find that they increase $j_{\rm stars}(r_{50})$ in ≈70 per cent of the cases, by ≈44 per cent on average, and thus, this form of merger is the most efficient at spinning up galaxies. In the case of dry mergers, we do not find a strong dependence on any of the orbital parameters studied here.

When studying $j_{\rm stars}(5r_{50})$ (Fig. C2) we find very similar results. The only major difference is that dry mergers show a stronger dependence on the orbital parameters, with high $j_{\rm orbital}/j_{\rm stars}(5r_{50})$ and coplanar mergers leading to a higher fraction of galaxies displaying and increase in $j_{\rm stars}(5r_{50})$. Thus, we conclude that the AM in the inner parts of galaxies during dry mergers is not greatly affected by the orbital parameters of the mergers, but when focusing on the total $j_{\rm stars}$, we see that perpendicular and low $j_{\rm orbital}/j_{\rm stars}(5r_{50})$ mergers are the most catastrophic.

We conclude that in EAGLE wet, corotating mergers can spin up galaxies very efficiently, and even more if they have a high $j_{\rm orbital}/j_{\rm stars}(5r_{50})$. On the contrary, dry, counter-rotating mergers are the most effective in spinning down galaxies. The environment in which these mergers take place may have a significant impact. We find that wet mergers generally happen in haloes of higher spins compared to the median of all haloes. This could be interpreted as accretion spinning up haloes, as well as making the galaxies gas-rich and resulting in a high spin merger remnant. The consequences of such correlation are very interesting but beyond the scope of this paper, so we defer it to future investigation.

3.3 Rearrangement of $j_{\rm stars}$ during galaxy mergers

In Fig. 12, we study the mean radial $j_{\rm stars}$ profile of the primary galaxy before and after the merger in two bins of stellar mass and for minor/major mergers that are wet/dry. '*Before*' the merger here means the last snapshot in which the galaxy participating in the

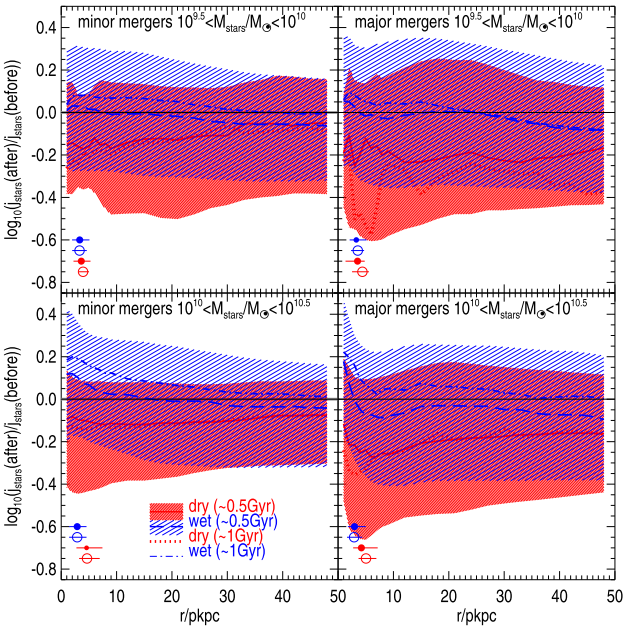

Figure 12. The ratio between the mean radial $j_{\rm stars}$ profiles after and before the galaxy merger, measured in an aperture r, as a function of r. We measure $j_{\rm stars}$ post-merger in the snapshot right after the merger, and two snapshots after, which correspond approximately to 0.5 and 1 Gyr after the merger, respectively. Minor and major mergers are shown in the left- and right-hand panels, respectively, in two bins of the neutral gas fraction of the merger, as labelled. The top panels show galaxies with $10^{9.5}\,{\rm M}_\odot < {\rm M}_{\rm stars} < 10^{10}\,{\rm M}_\odot$, while the bottom panels show galaxies with $10^{10}\,{\rm M}_\odot < {\rm M}_{\rm stars} < 10^{10.5}\,{\rm M}_\odot$. Lines and the shaded regions show the median and the 25th–75th percentile ranges. The latter are calculated using the snapshots right after the merger. The filled and open circles with the error bar at the bottom of each panel show the median r_{50} before and after the merger, respectively, for each sample and the 25th–75th percentile range, respectively. Horizontal lines mark no change in $j_{\rm stars}(r)$, and so values above (below) correspond to $j_{\rm stars}$ increasing (decreasing). The figure reveals that wet mergers tend to increase $j_{\rm stars}$ in the inner regions of galaxies, while decreasing it in the outer regions.

merger was individually identified, and for '*after*' the merger, we look at the two consecutive snapshots in which the galaxies has been identified as one (i.e. already merged in the merger tree). Given the time period in between snapshots, the two consecutive snapshots roughly correspond to ≈0.5 and ≈1 Gyr, respectively, after the merger. We study two snapshots after the merger because visual inspection of mergers in EAGLE reveals that in some cases the merger tree algorithm considers a galaxy pair as already merged even though the process is still ongoing. Another motivation to study two consecutive snapshots after the merger is to test the effect of relaxation if any is present.

In the low stellar mass bin of Fig. 12, we show that both dry minor and major mergers have the effect of reducing $j_{\rm stars}$ across the entire radii range considered. Studying $j_{\rm stars}$ at ≈0.5 or ≈1 Gyr after the merger makes little difference in this case. Major dry mergers tend to reduce $j_{\rm stars}$ by ≈0.2 dex on average in both low and high stellar mass bins, while minor dry mergers drive a more modest reduction of ≈0.1 dex, on average. In the case of wet mergers, we see a differential effect on the $j_{\rm stars}$ profiles: inner regions of galaxies, $r \lesssim 5$ kpc (typically $\approx 2\,r_{50}$; see filled and open circles in Fig. 12), tend to increase $j_{\rm stars}$, while at larger radii, $j_{\rm stars}$ tends to decrease if one looks at the merger remnant ≈0.5 Gyr after the merger, or very modestly increase if studied ≈1 Gyr after. The latter could be due

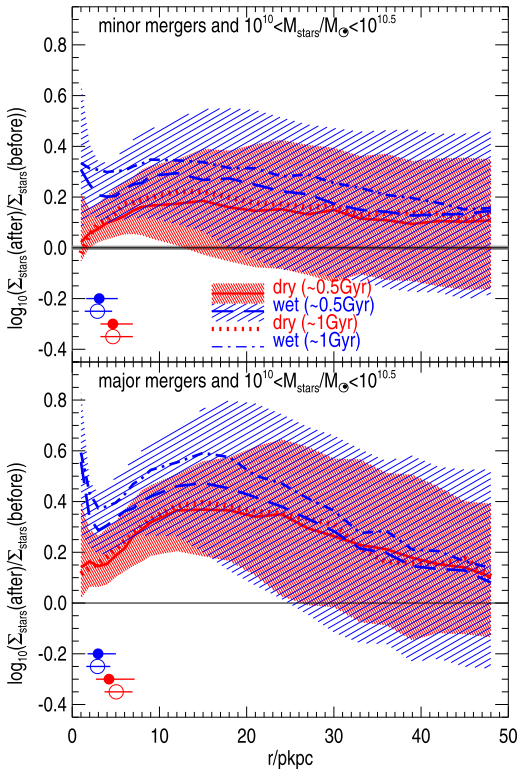

Figure 13. Stellar mass surface density profile before and after the mergers for the galaxies in the bottom panel of Fig. 12. This figure shows that gas-rich mergers tend to build the central stellar mass concentration (i.e. bulge), while dry mergers increase the stellar mass density towards the outskirts of galaxies. The latter case usually drives an increase in r_{50}, while the former does not change r_{50} significantly.

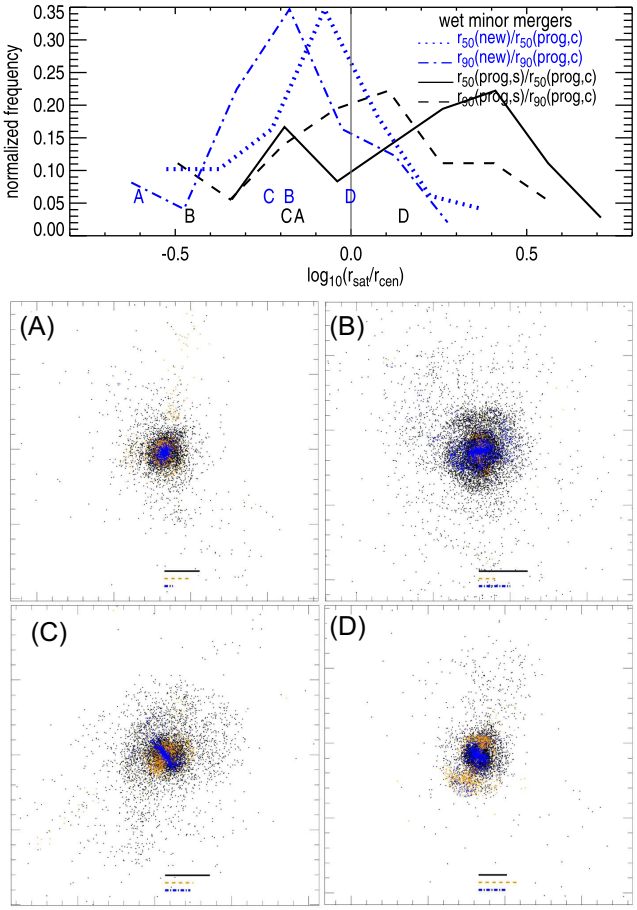

Figure 14. Top panel:the ratio between the 50 per cent and 90 per cent stellar mass radii of the progenitor satellite (labelled as 'prog,s') and the newly formed stars versus the progenitor central stellar (labelled as 'prog,c') components, as labelled, in all wet minor mergers in the redshift range ≈0.2–0.8 and that took place in primary galaxies with $M_{stars} \geq 10^{9.5}$ $M_\odot$ in EAGLE. This figure shows that newly formed stars reside in the centre of the galaxy and are more concentrated than the stars that were in primary galaxy before the merger. Bottom panel: stellar-particle distribution in four examples of wet major mergers that span the range of size ratios shown in the top panel. The images are *x*–*y* projections of 200 ckpc on a side. Black, yellow and blue points show progenitor stars that belonged to the primary galaxy, progenitor stars that belonged to the secondary galaxy and stars that formed during the merger, respectively. The segments of the same colours at the bottom show r_{90} of the three components.

to a combination of relaxation and continuing gas accretion and star formation. Separating the latter is not obvious in a simulation like EAGLE where all the physical processes are interplaying at any given time.

3.3.1 The physical origin of the j_{stars} *increase in wet mergers*

To further understand the differential effect wet mergers have on the mean radial j_{stars} profile, we study in Fig. 13 the change in the stellar surface density of the primary galaxy before and after the merger. For clarity, we only plot the mass bin 10^{10} $M_\odot$ < M_{stars} < $10^{10.5}$ $M_\odot$ as the lower mass bin gives very similar results. Fig. 13 shows that wet major and minor mergers drive a significant increase in the central stellar surface density by a factor $\gtrsim$0.2 dex, on average. At intermediate radii 5 pkpc $\lesssim r \lesssim$ 30 pkpc, there is also an increase, but of a less significant magnitude. If the central stellar mass (i.e. bulge) is increasing and the rotational velocity increases as $v \approx \sqrt{GM/r}$, j_{stars} is also expected to increase. This effect has been seen before in non-cosmological simulations of gas-rich mergers (Springel 2000; Cox et al. 2006; Robertson et al. 2006; Johansson et al. 2009; Peirani et al. 2010; Moreno et al. 2015).

One remaining question is whether the build-up of the bulge is driven by a preferential deposition of the stars of the satellite galaxy in the centre, by dynamical friction moving stars of the primary galaxy to the centre, or the preferential formation of new stars in the centre. To answer this question, we identified in the merger remnant the stars that belonged to the secondary (i.e. progenitor satellite stars) and primary (i.e. progenitor central stars) galaxy before the merger, and those that formed during the merger (i.e. new stars), and calculate their 50 per cent and 90 per cent stellar mass radii. We do this for all mergers that took place in the redshift range ≈0.2–0.8, which is of particular interest, as it is the time when the universe goes from being dominated by wet to dry mergers in EAGLE (see Fig. 2). Fig. 14 shows the ratio of r_{50} and r_{90} between the progenitor satellite stars and the progenitor central stars, and between the new stars and the progenitor central stars in the case of wet minor mergers. For the new stars, we find that in ≈73 per cent of cases they end up more concentrated and with r_{50} and r_{90} typically ≈1.3 times smaller than the progenitor central stars. For the progenitor satellite stars, we find that in ≈70 per cent of the cases, they end up more extended and with r_{50} and r_{90} values that are ≈1.8 and ≈1.3 times larger than those of the progenitor central stars. The bottom panel of Fig. 14 shows four examples of wet minor merger remnants and how the stars from the three components above are spatially

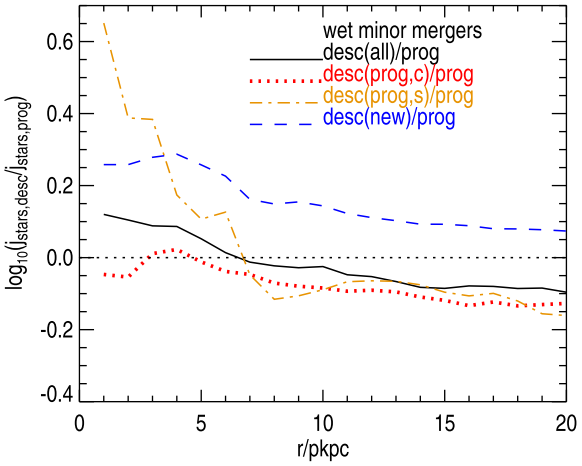

Figure 15. The ratio between the mean radial $j_{\rm stars}$ profiles after and before the galaxy merger (solid line), measured in an aperture r, as a function of r, for all wet minor mergers in the redshift range ≈0.2–0.8 and that took place in primary galaxies with $M_{\rm stars} \geq 10^{9.5}$ M$_\odot$ in EAGLE. We also show the ratio between the mean radial $j_{\rm stars}$ profiles of the descendant and the progenitor but when we measure the former only with the progenitor central (dotted line), progenitor satellite (dot–dashed line) and newly formed stars (dashed line). Here, lines show the medians. This figure shows that the increase in $j_{\rm stars}$ in a wet merger is due to the contribution of newly formed stars.

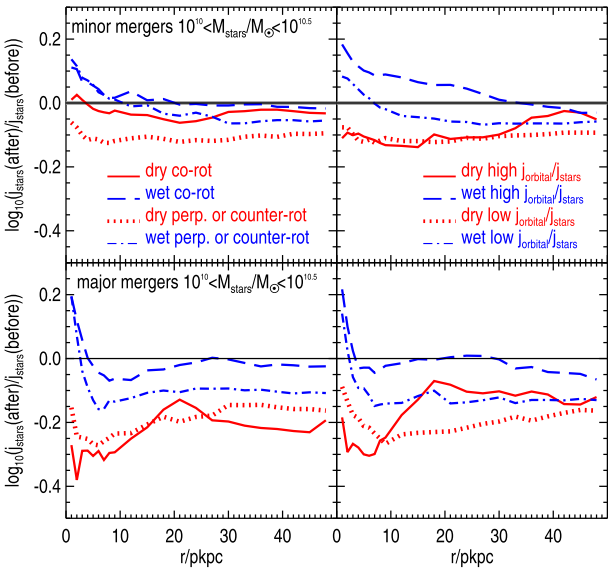

Figure 16. The ratio between the mean radial $j_{\rm stars}$ profiles after and before the galaxy merger, measured in an aperture r, as a function of r for galaxies with stellar masses in the range 10^{10} M$_\odot$ < M$_{\rm stars}$ < $10^{10.5}$ M$_\odot$ at $z < 2$. Mergers are split into minor (top panels) and major (bottom panels). In addition, every panel shows wet and dry mergers as red and blue lines split into corotating versus perpendicular or counter-rotating mergers (left-hand panels) and high versus low $j_{\rm orbital}/j_{\rm stars}$ (right-hand panels), as labelled. Here, we study consecutive snapshots, which in practice means that the profile *after* the merger is measured at ≈0.3–0.5 Gyr after the merger. Lines correspond to the medians of the distributions. For clarity, we do not show here the percentile ranges, but they are of a similar magnitude to those shown in Fig. 12.

distributed. We generally find that when r_{50} of the progenitor satellite stars is larger than that of the progenitor central stars, there is an associated extended stellar structure in the form of streams or shells (e.g. galaxy 'D' in Fig. 14). If we focus on the central 2 pkpc, we find that the bulge mass is dominated by the progenitor central stars (≈70 per cent on average), but with a large contribution from the newly formed stars (≈30 per cent on average). Although there is a significant contribution of newly formed stars, we find that the mass-weighted age of the bulge by $z = 0$ is $\gtrsim$9.5 Gyr old, on average, due to the stars contributed by the primary and secondary galaxies that end up in the central 2 pkpc being extremely old.

We also studied the contribution of these stars to the mean $j_{\rm stars}$ radial profile of the merger remnant in the inner 20 pkpc in Fig. 15. We find that the increase in $j_{\rm stars}$ in the inner regions of galaxies as a result of the wet merger and reported in Fig. 12 is due to the newly formed stars. Although the progenitor satellite stars also have a high $j_{\rm stars}$ compared to the progenitor central stars, their contribution to the stellar mass is very small. In fact, in the inner 2 pkpc, newly formed stars are responsible for 33 per cent of the $j_{\rm stars}$ of the descendant, while progenitor central and satellite stars contribute 58 per cent and 9 per cent, respectively, on average. At larger radii, $j_{\rm stars}$ of the descendant is dominated by the stars of the progenitor central galaxy.

The main difference between wet minor and major mergers is that in the latter (not shown here) the stars belonging to the progenitor secondary galaxy end up more concentrated than the primary progenitor central stars (typically ≈1.5 times more concentrated, on average).

We conclude that the increase of $j_{\rm stars}$ in the inner regions of galaxies as a result of a wet merger is caused primarily by the flows of gas towards the centre that subsequently form stars. These new stars contribute to the formation of the bulge and are typically characterized by higher j at fixed radius, thus producing steeper velocity profiles.

3.3.2 *The effect of spin and orbital alignments*

In Fig. 16, we show the mean radial $j_{\rm stars}$ profiles of galaxies before and after the merger. After the merger corresponds to the first snapshot in which the two merging galaxies are identified as one single remnant (typically 0.5 Gyr after the merger). In the left-hand panels of Fig. 16, we separate dry and wet minor (top) and major (bottom) mergers that took place in galaxies with 10^{10} M$_\odot$ < M$_{\rm stars}$ < $10^{10.5}$ M$_\odot$ into the subsamples of corotating (cos($\theta_{\rm spin}$) > 0.7; see equation 2 for a definition of $\theta_{\rm spin}$), and perpendicular or counter-rotating galaxies (cos($\theta_{\rm spin}$) < 0.15).

Wet minor mergers of galaxies that are spin up the central region, due to the build-up of the bulge, and have very little effect on the outskirts of the galaxy [i.e. $j_{\rm stars}$(after) ∼ j$_{\rm stars}$(before)]. In the case of perpendicular or counter-rotating galaxies, there is a significant spin-down at $r \gtrsim 10$ pkpc of ≈40 per cent, on average, in the case of major mergers, and a more modest one of ≈12 per cent for minor mergers. A very significant difference is seen in dry minor mergers between corotating or perpendicular/counter-rotating galaxies. We find that very little happens to $j_{\rm stars}(r)$ if the dry minor merger is between corotating galaxies, while in the case of perpendicular/counter-rotating mergers, there is a significant stripping of $j_{\rm stars}(r)$ of ≈30 per cent, on average, through the entire radii range studied here. Note that in the case of dry major mergers, there is always a significant stripping of $j_{\rm stars}$ regardless of the spin and orbital parameters.

In the right-hand panels of Fig. 16, we show the ratio between the mean radial $j_{\rm stars}$ profiles before and after the merger as a function of r for subsamples of dry/wet minor/major mergers, split

into two bins of $j_{\rm orbital}/j_{\rm stars}(5r_{50})$. These two bins are above [high $j_{\rm orbital}/j_{\rm stars}(5r_{50})$] and below [low $j_{\rm orbital}/j_{\rm stars}(5r_{50})$] the median value of $j_{\rm orbital}/j_{\rm stars}(5r_{50})$. Here, $j_{\rm stars}(5r_{50})$ corresponds to the value of the primary galaxy prior to the merger. In Section 3.2, we show that this was the most important orbital parameter determining whether a galaxy suffered a spin-up or -down as a result of the merger. In the case of high $j_{\rm orbital}/j_{\rm stars}(5r_{50})$, we find that wet minor mergers result in a spin-up that is significant out to $r \approx 30$ pkpc, increasing $j_{\rm stars}(r)$ by ≈60 per cent at $r \lesssim 5$ pkpc and ≈25 per cent at 5 pkpc $\lesssim$ r $\lesssim$ 15 pkpc. Such a merger in EAGLE is the most effective at spinning up galaxies. These galaxies can end up in the upper envelope of the $j_{\rm stars}$–$M_{\rm stars}$ relation. For wet major mergers, we find a significant increase in the very inner regions ($r \lesssim$ 3 pkpc), and very little change at larger radii. Dry mergers show very little difference between high and low $j_{\rm orbital}/j_{\rm stars}(5r_{50})$, on average. Di Matteo et al. (2009) showed that in the case of very high $j_{\rm orbital}$, the remnant can end up with a large $j_{\rm stars}$ even in the case of dry mergers. EAGLE reveals that this type of event is very rare, and most of the time the galaxies spin down as a result of a dry merger.

In the case of low $j_{\rm orbital}/j_{\rm stars}(5r_{50})$, wet mergers show modest to large losses of $j_{\rm stars}(<r)$. This large difference between the high/low $j_{\rm orbital}/j_{\rm stars}(5r_{50})$ subsamples arise from the efficient transfer of $j_{\rm orbital}$ on to the remnant galaxy, which can significantly spin up a galaxy when $j_{\rm orbital}$ is large.

4 DISCUSSION AND CONCLUSIONS

The classic interpretation of the positions of spiral and elliptical galaxies in the $j_{\rm stars}$–$M_{\rm stars}$ plane by, e.g. Fall (1983) and Romanowsky & Fall (2012) says that spiral galaxies are the result of weak conservation of specific AM of the gas falling in and forming stars, while elliptical galaxies lose ≳50–90 per cent of their j during their formation process. The preferred invoked mechanism responsible for such loss is galaxy mergers.

While we find mergers to preferentially spin galaxies down, their influence can be quite varied, and in many cases, they spin galaxies up significantly, positioning them in the upper envelope of the $j_{\rm stars}$–stellar mass relation. The latter is the case of wet mergers between corotating galaxies and with high $j_{\rm orbital}$ relative to the $j_{\rm stars}$ of the galaxies prior to the merger. When studying the correlation between the positions of galaxies in the $j_{\rm stars}$–stellar mass plane and their merger history, we find the wet merger rate increases with decreasing stellar mass and increasing $j_{\rm stars}$, while the dry merger rate increases with increasing stellar mass and decreasing $j_{\rm stars}$. In fact, EAGLE shows that for the $j_{\rm stars}$ value of the merger remnant galaxy, the most important parameter is the gas fraction of the merger, rather than the mass ratio or the spin/orbital parameters. The latter play a secondary, none the less relatively important, role. Dry mergers are the most effective way of spinning down galaxies, though the subsample of minor, corotating mergers are relatively harmless. Counter-rotating dry mergers are the most efficient at spinning galaxies down. Our definition of wet and dry is very gas-rich and gas-poor. Thus, dry mergers may be slightly different than the purely collisionless experiments widely discussed in the literature (e.g. Boylan-Kolchin, Ma & Quataert 2005; Naab, Khochfar & Burkert 2006b; Taranu et al. 2013; Naab et al. 2014).

Classical results of dry mergers by early works (e.g. Barnes & Efstathiou 1987; Navarro, Frenk & White 1997) show that dynamical friction redistributes $j_{\rm stars}$ in a way such that most of it ends up at very large radii, but if integrating over a large enough baseline, one finds $j_{\rm stars}$ converging to $j_{\rm halo}$. These results were refuted by the observations of elliptical galaxies compiled by Romanowsky & Fall (2012); these authors showed in a sample of seven early-type galaxies that some of them converged in their $j_{\rm stars}$ to values that would indicate a large deficiency compared to an average $j_{\rm halo}$. Using EAGLE, we found that dry merger remnants, those with the highest Sérsic indices, have most of their $j_{\rm stars}$ budget at $r \gtrsim 5 \times r_{50}$, in agreement with the early works discussed above, but that the variety of the radial $j_{\rm stars}$ profiles of galaxies, particularly at low $j_{\rm stars}(r_{50})$, can easily explain the rotation curves presented in Romanowsky & Fall (2012). We compared the EAGLE $j_{\rm stars}$ profiles with ATLAS$^{\rm 3D}$ galaxies and found excellent agreement. The main difference between what we find with EAGLE and the early papers above is that the total $j_{\rm stars}$ in the case of dry merger remnants converges to ≈20 per cent of the halo j, on average, while galaxies that never had a merger of the same stellar mass, typically have a total $j_{\rm stars}$ that is ≈40 per cent of their $j_{\rm halo}$. Thus, a relatively modest but significant difference is found between these two samples.

The case of wet mergers in EAGLE is very interesting from the perspective of $j_{\rm stars}$ and the morphology of galaxies. We find that in most of these mergers, the inner regions of galaxies undergo a spin-up as a result of stars being formed in the central ≈2–5 pkpc with high circular velocities. These newly formed stars are the result of gas inflows triggered by the merger and drive the build-up of the bulge. These new stars display a significantly more concentrated distribution compared to the stars that were present in the primary or the secondary galaxy before the merger. Stars that belonged to the secondary galaxy end up preferentially more concentrated than the stars of the primary galaxy in the case of major mergers, and significantly more extended in the case of minor mergers. These extended structures are in the form of streams and/or shells.

Key observational tests to support our findings for the effect of mergers on the $j_{\rm stars}$ of elliptical galaxies would be to increase the sample of elliptical galaxies with good kinematic information out to $10\,r_{50}$. Our predictions are as follows: (i) The mean radial $j_{\rm stars}$ profiles of ellipticals are typically shallower than spiral galaxies and that (ii) these profiles continue to rise well beyond $10\,r_{50}$. A cautionary note: Many of these stars that are beyond $10\,r_{50}$ would not necessarily be considered part of the galaxy, but instead they may belong to the stellar halo. In terms of the mean radial $j_{\rm stars}$ profile, however, we do not see obvious features that would indicate distinct stellar components.

A plausible strategy to test the raising $j_{\rm stars}$ profiles of ellipticals would be to use IFU surveys, such as SAMI and MaNGA, to define a suitable sample of galaxies, selected from the $j_{\rm stars}$–stellar mass plane, with $j_{\rm stars}$ here measured within some relatively small aperture (e.g. SAMI used one effective radius to measure $j_{\rm stars}$ within; Cortese et al. 2016), and follow up to measure $j_{\rm stars}$ out to radii $>10\,r_{50}$. The latter can be achieved by studying the kinematics of planetary nebulae and/or globular clusters (e.g. Coccato et al. 2009; Romanowsky et al. 2009; McNeil et al. 2010; Foster et al. 2011). In addition, the lack of information on the 3D stellar densities and velocities makes it necessary to develop fitting tools that enable the reconstruction of 3D galaxies by imposing Newtonian constraints on IFU data. Observations and modelling tools like the ones described here would provide stringent constraints to the simulation and the galaxy formation physics included in it.

ACKNOWLEDGEMENTS

We thank Luca Cortese and Matthieu Schaller for useful discussions and comments on the manuscript. CL is funded by a Discovery Early Career Researcher Award (DE150100618). CL also

thanks the MERAC Foundation for a Postdoctoral Research Award. This work was supported by a Research Collaboration Award at the University of Western Australia. This work used the DiRAC Data Centric system at Durham University, operated by the Institute for Computational Cosmology on behalf of the STFC DiRAC HPC Facility (www.dirac.ac.uk). This equipment was funded by BIS National E-infrastructure capital grant ST/K00042X/1, STFC capital grant ST/H008519/1, and STFC DiRAC Operations grant ST/K003267/1 and Durham University. DiRAC is part of the National E-Infrastructure. Support was also received via the Interuniversity Attraction Poles Programme initiated by the Belgian Science Policy Office ([AP P7/08 CHARM]), the National Science Foundation under Grant No. NSF PHY11-25915 and the UK Science and Technology Facilities Council (grant numbers ST/F001166/1 and ST/I000976/1) via rolling and consolidating grants awarded to the ICC. We acknowledge the Virgo Consortium for making their simulation data available. The EAGLE simulations were performed using the DiRAC-2 facility at Durham, managed by the ICC, and the PRACE facility Curie based in France at TGCC, CEA, Bruyeres-le-Chatel. This research was supported in part by the National Science Foundation under Grant No. NSF PHY11-25915. Parts of this research were conducted by the Australian Research Council Centre of Excellence for All-sky Astrophysics (CAASTRO), through project number CE110001020, and supported by the Australian Research Council Discovery Project 160102235.

REFERENCES

Abadi M. G., Navarro J. F., Steinmetz M., Eke V. R., 2003, ApJ, 597, 21
Bacon R. et al., 2010, in McLean I. S., Ramsay S. K., Takami H., eds, Proc. SPIE Conf. Ser. Vol. 7735, Ground-based and Airborne Instrumentation for Astronomy III. SPIE, Bellingham, p. 773508
Bahé Y. M. et al., 2016, MNRAS, 456, 1115
Barnes J. E., 1988, ApJ, 331, 699
Barnes J., Efstathiou G., 1987, ApJ, 319, 575
Baugh C. M., 2006, Rep. Prog. Phys., 69, 3101
Bekki K., 1998, ApJ, 502, L133
Bluck A. F. L., Conselice C. J., Bouwens R. J., Daddi E., Dickinson M., Papovich C., Yan H., 2009, MNRAS, 394, L51
Bluck A. F. L., Conselice C. J., Buitrago F., Grützbauch R., Hoyos C., Mortlock A., Bauer A. E., 2012, ApJ, 747, 34
Bois M. et al., 2011, MNRAS, 416, 1654
Bower R. G., Benson A. J., Malbon R., Helly J. C., Frenk C. S., Baugh C. M., Cole S., Lacey C. G., 2006, MNRAS, 370, 645
Boylan-Kolchin M., Ma C.-P., Quataert E., 2005, MNRAS, 362, 184
Bundy K., Fukugita M., Ellis R. S., Targett T. A., Belli S., Kodama T., 2009, ApJ, 697, 1369
Bundy K. et al., 2015, ApJ, 798, 7
Burkert A. et al., 2016, ApJ, 826, 214
Cappellari M. et al., 2011, MNRAS, 413, 813
Coccato L. et al., 2009, MNRAS, 394, 1249
Cole S., Lacey C. G., Baugh C. M., Frenk C. S., 2000, MNRAS, 319, 168
Correa C. A., Schaye J., Clauwens B., Bower R. G., Crain R. A., Schaller M., Theuns T., Thob A. C. R., 2017, MNRAS, 472, L45
Cortese L. et al., 2016, MNRAS, 463, 170
Cox T. J., Dutta S. N., Di Matteo T., Hernquist L., Hopkins P. F., Robertson B., Springel V., 2006, ApJ, 650, 791
Crain R. A. et al., 2015, MNRAS, 450, 1937 (C15)
Crain R. A. et al., 2017, MNRAS, 464, 4204
Croom S. M. et al., 2012, MNRAS, 421, 872
De Lucia G., Springel V., White S. D. M., Croton D., Kauffmann G., 2006, MNRAS, 366, 499
Di Matteo P., Jog C. J., Lehnert M. D., Combes F., Semelin B., 2009, A&A, 501, L9
Dolag K., Borgani S., Murante G., Springel V., 2009, MNRAS, 399, 497
Dubois Y. et al., 2014, MNRAS, 444, 1453
Dubois Y., Peirani S., Pichon C., Devriendt J., Gavazzi R., Welker C., Volonteri M., 2016, MNRAS, 463, 3948
Emsellem E. et al., 2007, MNRAS, 379, 401
Emsellem E. et al., 2011, MNRAS, 414, 888
Fall S. M., 1983, in Athanassoula E., ed., Proc. IAU Symp. 100, Internal Kinematics and Dynamics of Galaxies. Reidel, Dordrecht, p. 391
Fall S. M., Romanowsky A. J., 2013, ApJ, 769, L26
Farouki R. T., Shapiro S. L., 1982, ApJ, 259, 103
Foster C. et al., 2011, MNRAS, 415, 3393
Furlong M. et al., 2015, MNRAS, 450, 4486
Furlong M. et al., 2017, MNRAS, 465, 722
Genel S., Fall S. M., Hernquist L., Vogelsberger M., Snyder G. F., Rodriguez-Gomez V., Sijacki D., Springel V., 2015, ApJ, 804, L40
Harrison C. M. et al., 2017, MNRAS, 467, 1965
Hearin A. P., Behroozi P. S., van den Bosch F. C., 2016, MNRAS, 461, 2135
Heyl J. S., Hernquist L., Spergel D. N., 1996, ApJ, 463, 69
Jesseit R., Cappellari M., Naab T., Emsellem E., Burkert A., 2009, MNRAS, 397, 1202
Jiang L., Helly J. C., Cole S., Frenk C. S., 2014, MNRAS, 440, 2115
Johansson P. H., Naab T., Burkert A., 2009, ApJ, 690, 802
Kauffmann G., Li C., Zhang W., Weinmann S., 2013, MNRAS, 430, 1447
Lagos C. D. P., Cora S. A., Padilla N. D., 2008, MNRAS, 388, 587
Lagos C. d. P. et al., 2015, MNRAS, 452, 3815
Lagos C. d. P. et al., 2016, MNRAS, 459, 2632
Lagos C. d. P., Theuns T., Stevens A. R. H., Cortese L., Padilla N. D., Davis T. A., Contreras S., Croton D., 2017, MNRAS, 464, 3850
López-Sanjuan C. et al., 2012, A&A, 548, A7
Lotz J. M., Jonsson P., Cox T. J., Primack J. R., 2010, MNRAS, 404, 590
McAlpine S. et al., 2016, Astron. Comput., 15, 72
McNeil E. K., Arnaboldi M., Freeman K. C., Gerhard O. E., Coccato L., Das P., 2010, A&A, 518, A44
Makino J., Hut P., 1997, ApJ, 481, 83
Mo H. J., Mao S., White S. D. M., 1998, MNRAS, 295, 319
Moreno J., Torrey P., Ellison S. L., Patton D. R., Bluck A. F. L., Bansal G., Hernquist L., 2015, MNRAS, 448, 1107
Naab T., Jesseit R., Burkert A., 2006a, MNRAS, 372, 839
Naab T., Khochfar S., Burkert A., 2006b, ApJ, 636, L81
Naab T. et al., 2014, MNRAS, 444, 3357
Navarro J. F., White S. D. M., 1994, MNRAS, 267, 401
Navarro J. F., Frenk C. S., White S. D. M., 1997, ApJ, 490, 493
Obreschkow D., Glazebrook K., 2014, ApJ, 784, 26
Pakmor R., Springel V., Bauer A., Mocz P., Munoz D. J., Ohlmann S. T., Schaal K., Zhu C., 2016, MNRAS, 455, 1134
Pedrosa S. E., Tissera P. B., 2015, A&A, 584, A43
Peirani S., Crockett R. M., Geen S., Khochfar S., Kaviraj S., Silk J., 2010, MNRAS, 405, 2327
Planck Collaboration XVI, 2014, A&A, 571, A16
Qu Y. et al., 2017, MNRAS, 464, 1659
Robertson B., Bullock J. S., Cox T. J., Di Matteo T., Hernquist L., Springel V., Yoshida N., 2006, ApJ, 645, 986
Robotham A. S. G. et al., 2014, MNRAS, 444, 3986
Rodriguez-Gomez V. et al., 2017, MNRAS, 467, 3083
Romanowsky A. J., Fall S. M., 2012, ApJS, 203, 17
Romanowsky A. J., Strader J., Spitler L. R., Johnson R., Brodie J. P., Forbes D. A., Ponman T., 2009, AJ, 137, 4956
Sales L. V., Navarro J. F., Schaye J., Dalla Vecchia C., Springel V., Booth C. M., 2010, MNRAS, 409, 1541
Scannapieco C. et al., 2012, MNRAS, 423, 1726
Schaller M. et al., 2015a, MNRAS, 451, 1247
Schaller M., Dalla Vecchia C., Schaye J., Bower R. G., Theuns T., Crain R. A., Furlong M., McCarthy I. G., 2015b, MNRAS, 454, 2277
Schaye J. et al., 2015, MNRAS, 446, 521 (S15)
Serra P. et al., 2012, MNRAS, 422, 1835
Sokolowska A., Capelo P. R., Fall S. M., Mayer L., Shen S., Bonoli S., 2017, ApJ, 835, 289
Sparre M., Springel V., 2016, MNRAS, 462, 2418

Sparre M., Springel V., 2017, MNRAS, 470, 3946
Springel V., 2000, MNRAS, 312, 859
Springel V., 2005, MNRAS, 364, 1105
Springel V., White S. D. M., Tormen G., Kauffmann G., 2001, MNRAS, 328, 726
Springel V. et al., 2008, MNRAS, 391, 1685
Stevens A. R. H., Croton D. J., Mutch S. J., 2016, MNRAS, 461, 859
Stevens A. R. H., Lagos C. d. P., Contreras S., Croton D. J., Padilla N. D., Schaller M., Schaye J., Theuns T., 2017, MNRAS, 467, 2066
Swinbank A. M. et al., 2017, MNRAS, 467, 3140
Taranu D. S., Dubinski J., Yee H. K. C., 2013, ApJ, 778, 61
Teklu A. F. et al., 2015, ApJ, 812, 29
Toomre A., 1977, in Tinsley B. M., Larson D. Campbell R. B. G., eds, Evolution of Galaxies and Stellar Populations. Yale Univ. Obser., New Haven, p. 401
Toomre A., Toomre J., 1972, ApJ, 178, 623
Trayford J. W. et al., 2015, MNRAS, 452, 2879
Veale M. et al., 2017, MNRAS, 464, 356
Vogelsberger M. et al., 2014, MNRAS, 444, 1518
Wang J. et al., 2015, MNRAS, 453, 2399
Welker C., Dubois Y., Pichon C., Devriendt J., Chisari E. N., 2015, A&A, preprint (arXiv:1512.00400)
White S. D. M., 1978, MNRAS, 184, 185
White S. D. M., Rees M. J., 1978, MNRAS, 183, 341
Young L. M. et al., 2011, MNRAS, 414, 940
Zavala J., Okamoto T., Frenk C. S., 2008, MNRAS, 387, 364
Zavala J. et al., 2016, MNRAS, 460, 4466

APPENDIX A: CONVERGENCE TEST

We perform a 'strong' convergence[2] test (see S15 for a discussion on 'strong' and 'weak' convergences) of the resolution we use throughout this work (see Table 1). To do this, we use a smaller volume, but same resolution as the simulation described in Table 1, and a run with the same box size but higher resolution (see Table A1 for the details of the simulations). Schaller et al. (2015a) and Lagos et al. (2017) have already presented detailed convergence tests for the mass and velocity radial distribution of galaxies, and AM, respectively, in EAGLE. Here, we focus on the radial profiles of $j_{\rm stars}$ of galaxies in EAGLE that have (not) had mergers.

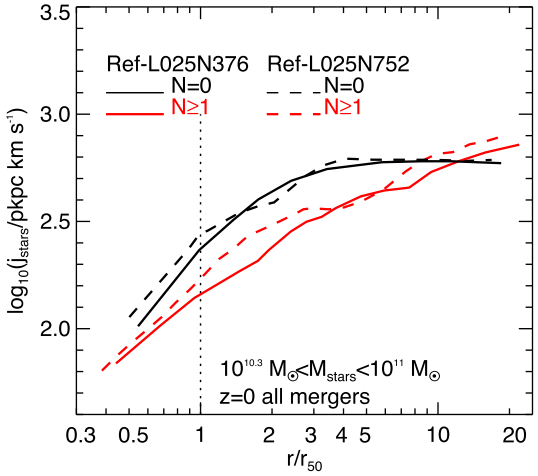

Figure A1. $j_{\rm stars}(r)$ as a function of r for galaxies with stellar masses in the range $10^{10.3}$ M$_\odot$ < M$_{\rm stars}$ < 10^{11} M$_\odot$ at $z = 0$ for the Ref-L025N0376 (solid lines) and Ref-L025N0752 (dashed lines) simulations. Lines show the median $j_{\rm stars}(r)$. The 16th–84th percentile ranges are similar to those shown in Fig. 7.

Fig. A1 shows the $j_{\rm stars}$ radial profiles of galaxies that have not gone through mergers ($N = 0$), and those that had at least one merger ($N \geq 1$) by $z = 0$ in EAGLE. The difference between the $N = 0$ and $N \geq 1$ is very similar in the two simulations despite their difference in resolution. This shows that the profiles analysed in this work are well converged at the resolution adopted in the simulation of Table 1.

[2] Strong convergence test refers to comparing simulations with the same subgrid physics and parameters, as well as volume and initial conditions, but with different resolutions.

Table A1. EAGLE simulations used in this appendix. The column list: (1) the name of the simulation, (2) comoving box size, (3) number of particles, (4) initial particle masses of gas and (5) dark matter, (6) comoving gravitational softening length and (7) maximum physical comoving Plummer-equivalent gravitational softening length. Units are indicated below the name of each column. EAGLE adopts (6) as the softening length at $z \geq 2.8$, and (7) at $z < 2.8$.

(1) Name Units	(2) L (cMpc)	(3) # particles	(4) Gas particle mass ($M_\odot$)	(5) DM particle mass ($M_\odot$)	(6) Softening length (ckpc)	(7) Max. gravitational softening (pkpc)
Ref-L025N0376	25	2×376^3	1.81×10^6	9.7×10^6	2.66	0.7
Ref-L025N0752	25	2×752^3	2.26×10^5	1.21×10^6	1.33	0.35

APPENDIX B: RADIAL $j_{\rm stars}$ PROFILES AT FINE TIME INTERVALS BETWEEN OUTPUTS

The standard trees of EAGLE connect 29 epochs for which snapshots are saved (including all particle properties). The time span between snapshots can range from ≈0.3 to ≈1 Gyr. Galaxy mergers, however, may require finer time intervals between snapshots to follow in more detail how the merger evolves. Schaye et al. (2015) showed that in addition to the snapshots described above, the EAGLE simulations also record 400 *snipshots*, in the redshift range $0 \leq z \leq 20$, saving fewer gas particle properties. In our case, we would like to measure the mean radial $j_{\rm stars}$ profile in galaxies during and after the merger, and the information stored in snipshots allows us to do this. Owing to the computational expense of applying SUBFIND to the outputs of EAGLE only 200 even-numbered snipshots of the simulation suite were catalogued. This decreases the time span between snipshots to ≈0.05 to 0.3 Gyr.

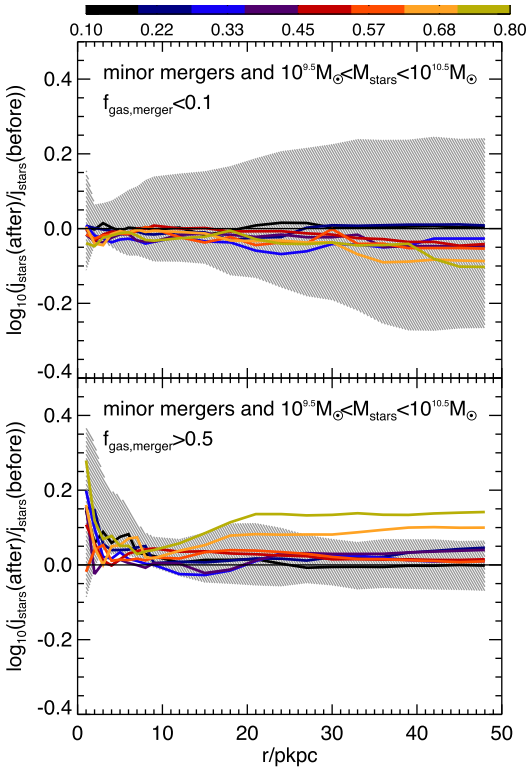

Figure B1. The ratio between the mean $j_{\rm stars}$ after and before galaxy mergers, measured in an aperture r, as a function of r. We measure $j_{\rm stars}$ after the merger in eight subsequent snipshots after the merger. Each snipshot samples a time-step of ≈0.1 Gyr. Here, we show galaxies with $10^{9.5}\,{\rm M}_\odot < {\rm M}_{\rm stars} < 10^{10.5}\,{\rm M}_\odot$ that went through a minor merger in the redshift range $0.65 \lesssim z \lesssim 0.75$. The top panel shows the subsample of gas-poor mergers, while the bottom panel shows gas-rich mergers. Lines show the median, with the colour indicating the time after the merger, as shown in the colour bar at the top. For simplicity, we only show the 25th–75th percentile range (shaded region) for the first snipshot after the merger. For reference, the horizontal lines show no change on $j_{\rm stars}(r)$, and so values above the line show an increase in $j_{\rm stars}$, while the opposite holds if below the line.

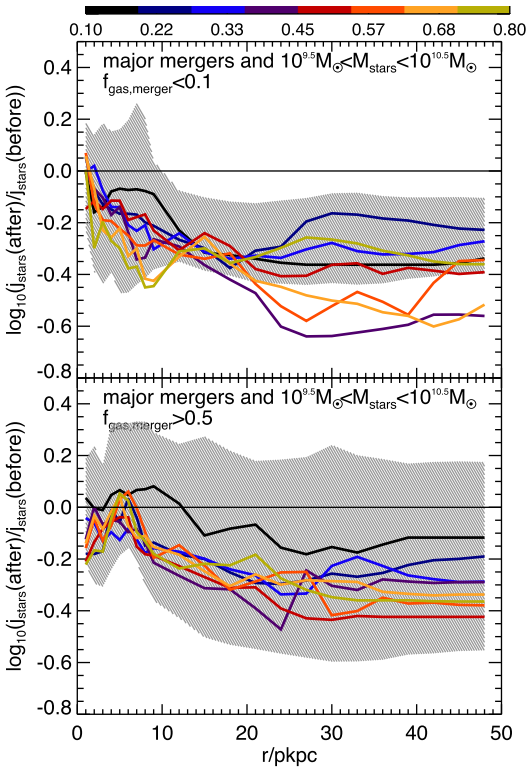

Figure B2. As Fig. B1 but for major mergers.

Here, we take all the snipshots between $z \approx 0.5$ and $z \approx 1$ and select all galaxy mergers that took place in that redshift range. We focus on this range because it is roughly when gas-rich and gas-poor mergers happen in similar numbers (see Fig. 2) in the Ref-L0100N1504 simulation. We calculate the radial $j_{\rm stars}$ profiles before and after the galaxy mergers (from ≈0.1 to ≈0.8 Gyr after a minor merger, in time-steps of ≈0.1 Gyr). We show in Fig. B1 the radial $j_{\rm stars}$ profiles after the merger divided by the profiles before the merger for galaxies with $10^{9.5}\,{\rm M}_\odot < {\rm M}_{\rm stars} < 10^{10.5}\,{\rm M}_\odot$ We separate mergers into gas-rich and gas-poor. Our idea here is to test if the results of Fig. 12 are affected by how fine the time interval between outputs is in the simulation. We find that gas-poor minor mergers systematically decrease $j_{\rm stars}$ over the entire radial range, while gas-rich minor mergers help increase $j_{\rm stars}$ in the central parts of galaxies, while changing only mildly $j_{\rm stars}$ at $r \gtrsim 10$ pkpc. Note that at later times (≳0.6 Gyr after the merger) $j_{\rm stars}$ in the

outer regions starts increasing faster. We interpret this behaviour as resulting from continuing star formation, rather than due to the galaxy merger.

Fig. B2 is as Fig. B1 but for major mergers. Although the trends are noisy, there is a systematic effect of gas-poor major mergers to decrease $j_{\rm stars}$ over the entire radial range probed here. Gas-rich major mergers tend to preferentially reduce $j_{\rm stars}$ at $r \gtrsim 10$ kpc, while not affecting the inner regions of galaxies much. Although noisy, one could even argue that $j_{\rm stars}$ increases in the inner regions of galaxies as a result of a gas-rich major merger. We find that the results here are broadly consistent with those presented in the top panels of Fig. 12, and thus, we conclude that finer time resolution only confirms the behaviour we analysed there.

APPENDIX C: THE EFFECT OF REDSHIFT, STELLAR MASS AND APERTURE IN $j_{\rm stars}$

In Section 3.2, we stacked all of the galaxy mergers that take place in galaxies with $M_{\rm stars} \geq 10^{9.5}$ M$_\odot$ and in the redshift range $0 \leq z \leq 2.5$. This may introduce significant biases due to the time-stepping

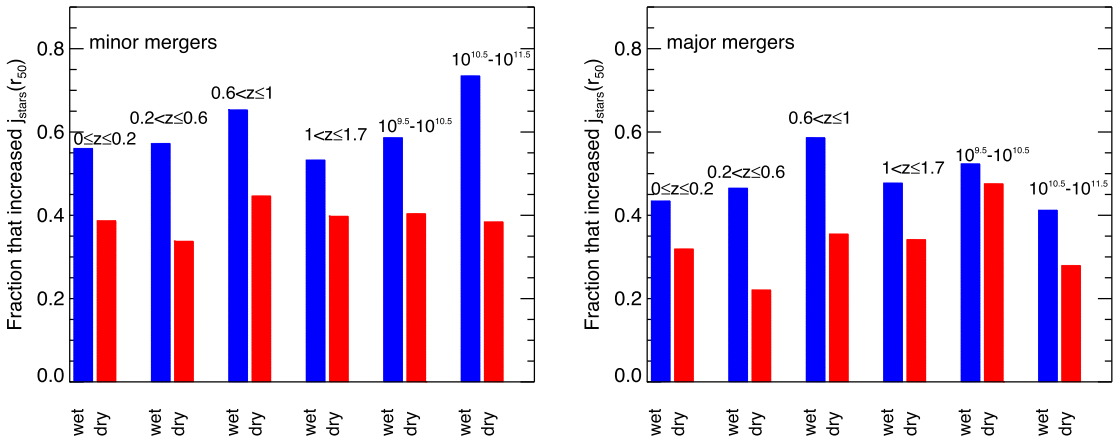

Figure C1. Left-hand panel:fraction of galaxies that display an increase in their $j_{\rm stars}(r_{50})$ during minor mergers at different redshifts and in two bins of stellar mass, split into wet and dry mergers, as labelled. Right-hand panel: as in the left-hand panel but for major mergers.

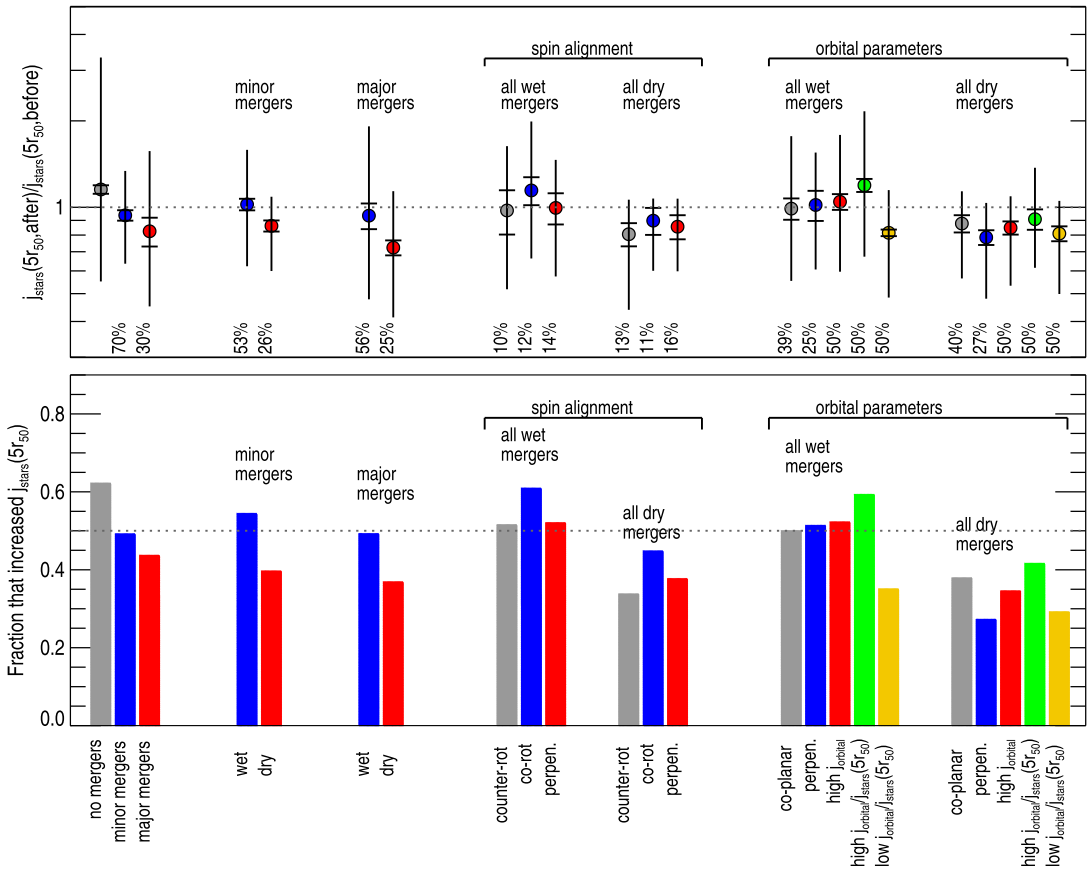

Figure C2. As Fig. 11 but for $j_{\rm stars}(5\,r_{50})$.

of the simulation (different snapshots cover different time-scales), and also due to galaxies having very different sizes at different cosmic epochs. In order to quantify that bias, we analyse galaxy mergers at different cosmic epochs and stellar mass bins, separated into minor and major and into wet and dry mergers in Fig. C1. We first compare the distributions as a function of gas richness, and we find that there is no statistical difference between the wet and dry minor merger populations at different redshifts. The KS p-values are in the range $\approx$0.2–0.9 when we compare wet or dry merger populations at different redshifts. When we compare wet versus dry minor mergers at different redshifts, we find that the differences seen in Fig. 11 are always present with high statistical significance (p-values are $\lesssim 10^{-4}$). When we analyse different stellar mass bins, we reach the same conclusion. Thus, we can comfortably assume that stacking minor mergers at different redshift does not introduce any significant bias to our analysis. In the case of major mergers, we see more variations between the subsamples at different redshifts and stellar masses, but the difference between dry and wet mergers is still the most important one statistically (with p-values $\lesssim 10^{-3}$).

Fig. C2 shows the ratio between $j_{\rm stars}(5\,r_{50})$ after and before mergers (top panel) and the frequency in which mergers increase $j_{\rm stars}(5r_{50})$ (bottom panel). We find that the results shown here are similar to those of Fig. 11 for $j_{\rm stars}$ measured within r_{50}.

This paper has been typeset from a TEX/LATEX file prepared by the author.